Available on CMS information server

CMS AN 2012/XXX

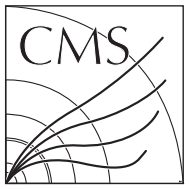

The Compact Muon Solenoid Experiment

Analysis Note

The content of this note is intended for CMS internal use and distribution only

February 13, 2012

Measurement of the WW Production Cross-section with the Full 2011 Dataset

L. Bauerdick, K. Burkett, I. Fisk, Y. Gao, O. Gutsche, B. Hooberman, S. Jindariani, S. Tkaczyk, V. Martinez Outschoorn

Fermilab National Accelerator Laboratory, Batavia, USA

G. Bauer, J. Bendavid, E. Butz, M. Chan, V. Dutta, G. Gómez-Ceballos, M. Goncharov, K. Hahn, P. Harris, M. Klute, S. Nahn, C. Paus, D. Ralph, F. Stoeckli, K. Sumorok, K. Sung, R. Wolf, S. Xie, M. Yang, M. Zanetti

Laboratory for Nuclear Science, Massachusetts Institute of Technology, Cambridge, USA

D. Barge, C. Campagnari, D. Kovalskyi, V. Krutelyov

University of California, Santa Barbara, Santa Barbara, USA

W. Andrews, G. Cerati, D. Evans, F. Golf, I. MacNeill, S. Padhi, Y. Tu, F. Würthwein, A. Yagil, J. Yoo

University of California, San Diego, San Diego, USA

I. Kravchenko

University of Nebraska-Lincoln, USA

Abstract

This note describes the WW cross-section measurement in 4.63 fb^{-1} of pp collision data at $\sqrt{s} = 7$ TeV with the CMS detector. The W leptonic decay channels with e, μ in the final state are considered. We find the cross-section to be $\sigma_{WW} = 53.41 \pm 2.03$ (stat.)± 4.28 (syst.)$\pm$ 2.40 (lumi.) pb.

Contents

1 Introduction

This note documents the W^+W^- production cross-section measurement in 4.63 fb^{-1} of pp collision data at $\sqrt{s} = 7$ TeV using leptonic decays, i.e. $W^+W^- \to \ell^+\nu\ell^-\bar{\nu}$, with electrons and muons in the final state. Fully leptonic tau decays are also considered as a part of the signal, but the selection requirements are not optimized for such events. The work is based on the selections and background estimation methods used in the Higgs boson search in the W^+W^- channel described in Ref. [8].

2 Data Samples

The datasets used for this analysis are summarized in Tables. 1 and 2 for data and Monte Carlo, respectively. The total integrated luminosity is 4.63 fb^{-1}. We used the official good run list [10]. For Monte Carlo simulation we use madgraph when possible, but different generators such as Pythia and Powheg are also used. For $gg \to W^+W^-$ a dedicated generator is used. For ZZ process we use Pythia, since MadGraph sample has a generator level cut on the dilepton invariant mass of 50 GeV.

Dataset Description	Dataset Name
$H \to W^+W^-$ Signal Selection Samples	
Run2011A MuEl PromptReco	/MuEG/Run2011A-PromptReco-v*/AOD
Run2011A DiMuon PromptReco	/DoubleMu/Run2011A-PromptReco-v*/AOD
Run2011A SingleMuon PromptReco	/SingleMu/Run2011A-PromptReco-v*/AOD
Run2011A DiElectron PromptReco	/DoubleElectron/Run2011A-PromptReco-v*/AOD
Run2011B DiElectron PromptReco	/DoubleElectron/Run2011B-PromptReco-v1/AOD
Run2011B DiMuon PromptReco	/DoubleMu/Run2011B-PromptReco-v1/AOD
Run2011B MuEl PromptReco	/MuEG/Run2011B-PromptReco-v1/AOD
Run2011B SingleMuon PromptReco	/SingleMu/Run2011B-PromptReco-v1/AOD
Run2011B SingleElectron PromptReco	/SingleElectron/Run2011B-PromptReco-v1/AOD
Fake Rate Measurement Samples	
Run2010A Jet PromptReco	/Jet/Run2011A-PromptReco-v*/AOD
Run2010B Jet PromptReco	/Jet/Run2011B-PromptReco-v*/AOD
Run2011A Photon PromptReco	/Photon/Run2011A-PromptReco-v4/AOD
Run2011B Photon PromptReco	/Photon/Run2011B-PromptReco-v1/AOD

Table 1: Summary of data datasets used.

With Pileup: Processed dataset name is always Summer11-PU_S4_START42_V11-v*/AODSIM		
Dataset Description	Primary Dataset Name	cross-section (pb)
qq $\to WW$	/WWJetsTo2L2Nu_TuneZ2_7TeV-madgraph-tauola	4.783
gg $\to WW \to 2l2\nu$	/GluGluToWWTo4L_TuneZ2_7TeV-gg2ww-pythia6	0.153
$t\bar{t}$	/TTTo2L2Nu2B_7TeV-powheg-pythia6/	157.5
t (s-chan)	/T_TuneZ2_s-channel_7TeV-powheg-tauola	3.19
$\bar{t}$ (s-chan)	/Tbar_TuneZ2_s-channel_7TeV-powheg-tauola	1.44
t (t-chan)	/T_TuneZ2_t-channel_7TeV-powheg-tauola	41.92
$\bar{t}$ (t-chan)	/Tbar_TuneZ2_t-channel_7TeV-powheg-tauola	22.65
tW	/T_TuneZ2_tW-channel-DR_7TeV-powheg-tauola	7.87
Z[20-inf] $\to ee$	/DYToEE_M-20_CT10_TuneZ2_7TeV-powheg-pythia	1666.0
Z[20-inf] $\to \mu\mu$	/DYToMuMu_M-20_CT10_TuneZ2_7TeV-powheg-pythia	1666.0
Z[20-inf] $\to \tau\tau$	/DYToTauTau_M-20_CT10_TuneZ2_7TeV-powheg-pythia-tauola	1666.0
Z[10-20] $\to ee$	/DYToEE_M-10To20_CT10_TuneZ2_7TeV-powheg-pythia	3892.9
Z[10-20] $\to \mu\mu$	/DYToMuMu_M-10To20_CT10_TuneZ2_7TeV-powheg-pythia	3892.9
Z[10-20] $\to \tau\tau$	/DYToTauTau_M-10To20_CT10_TuneZ2_7TeV-powheg-pythia-tauola	3892.9
W $\to \ell\nu$	/WJetsToLNu_TuneZ2_7TeV-madgraph-tauola	31314.0
WZ	/WZJetsTo3LNu_TuneZ2_7TeV-madgraph-tauola	0.857
ZZ	/ZZ_TuneZ2_7TeV_pythia6_tauola/	7.406
$W\gamma^* \to l\mu\mu$	/WGstarToLNu2Mu_TuneZ2_7TeV-madgraph-tauola	1.60
$W\gamma^* \to lee$	/WGstarToLNu2E_TuneZ2_7TeV-madgraph-tauola	5.55

Table 2: Summary of Monte Carlo datasets used..

3 Event Selection

The fully leptonic final state consists of two isolated leptons and large missing energy from the two undetectable neutrinos. The major reducible background processes are $\mathrm{t\bar{t}}$, W+jets and Drell-Yan. We thus perform several steps to select and extract the $\mathrm{W^+W^-}$ signal from data:

1. We select events that pass pre-defined lepton triggers.
2. We then select those events with two oppositely charged high p_T isolated leptons (ee, $\mu\mu$, $e\mu$) requiring:
   - $p_\mathrm{T} > 20$ GeV/c for both leptons;
   - standard identification and isolation requirements on both leptons.
3. We reject events with more than zero reconstructed jets;
4. large transverse missing energy due to the neutrinos.

The selection steps are now described in detail below.

3.1 Trigger

Triggering on $\mathrm{W^+W^-}$ decays in the dilepton final state increases in difficulty with increasing instantaenous luminosity. Single lepton triggers can only be sustained with very tight identification and isolation requirements and large transverse momentum thresholds. This means that double lepton triggers are the only viable option to maintain high signal efficiency.

We designed a suite of signal and control triggers appropriate for this analysis. These dilepton triggers have a high efficiency to collect $\mathrm{W^+W^-}$ events and are sufficiently loose to collect control events to estimate fake lepton backgrounds and selection efficiencies with adequate precision. The detailed trigger paths were described in [7].

3.2 Primary Vertex Reconstruction

Primary vertices are reconstructed using the so-called Deterministic Annealing clustering of tracks [13]. Reconstructed primary vertices are required to have a z position within 24 cm of the nominal detector center and a radial position within 2 cm of the beamspot. There must also be greater than four degrees of freedom in the fitted vertex. From the set of primary vertices in the event passing these selection cuts, the vertex with the largest summed squared-p_T of the associated tracks is chosen as the event primary vertex. Reconstructed leptons will be required to have small impact parameters with respect to this vertex.

3.3 Muon Selection

The muon selection is unchanged with respect to [7]. Muons in CMS are reconstructed as either $StandAloneMuons$ (track in the muon detector with low momentum resolution), $GlobalMuons$ (outside-in approach seeded by a $StandAloneMuon$ with a global fit using hits in the muon, silicon strip and pixel detectors) and $TrackerMuons$ (inside-out approach seeded by an offline silicon strip track, using the muon detector only for muon identification without refitting the track). Most good quality muons are reconstructed as all three types at the same time and the momentum resolution is dominated by the inner tracker system up to about 200 GeV/c in transverse momentum. We require the muon to be reconstructed as $GlobalMuon$, with $\chi^2/\mathrm{ndof} < 10$ on the global fit, must have at least one good muon hit, and at least two matches to muon segments in different muon stations; or $TrackerMuon$, provided it satisfies the "Tracker Muon Last Station Tight" selection requiring at least two muon segments matched at 3σ in local X and Y coordinates, with one being in the outermost muon station.

In addition, the following specific requirements to select good prompt isolated muons are the following:

- more than 10 hits in the inner tracker;

- at least one pixel hit;
- impact parameter in the transverse plane $|d_0| < 0.02$ (0.01) cm for muons with p_{T} greater (smaller) than 20 GeV/c, calculated with respect to the primary vertex;
- longitudinal impact parameter $|d_z| < 0.1$ cm, calculated with respect to the primary vertex;
- pseudorapidity $|\eta|$ must be smaller than 2.4;
- relative p_{T} resolution is better than 10%.
- decay in flight with the kink finding algorithm: $\chi^2/\mathrm{ndof} < 20$

Furthermore, the particle flow candidate-based isolation variable is used to reduce the contamination from the non-isolated muons originating from jets.

- $\mathrm{Iso}_{\mathrm{PF}}$: defined as the scalar sum of the p_{T} of the particle flow candidates satisfying the following requirements:
  - $\Delta R < 0.3$ to the muon in the $\eta \times \phi$ plane,
  - $|d_z(\mathrm{PFCandidate}) - d_z(\mathrm{muon})| < 0.1$ cm, if the PF candidate is charged,
  - $p_{\mathrm{T}} > 1.0$ GeV, if the PF candidate is classified as a neutral hadron or a photon.

We require $\frac{\mathrm{Iso}_{\mathrm{PF}}}{p_{\mathrm{T}}} < 0.13$ (0.06) for muons in the barrel with p_{T} greater (smaller) than 20 GeV/c. For muons in the endcap, we require $\frac{\mathrm{Iso}_{\mathrm{PF}}}{p_{\mathrm{T}}} < 0.09$ (0.05) for muons with p_{T} greater (smaller) than 20 GeV/c.

3.4 Electron Selection

We identify electrons using a multivariate approach optimized for this analysis [12]. In addition, we require some minimal requirements to make sure the electron candidate is as tight as the trigger selection:

- $p_T > 10$ GeV and $|\eta| < 2.5$
- $\sigma_{i\eta i\eta} < 0.01/0.03$ (barrel/endcap)
- $|\Delta\phi_{in}| < 0.15/0.10$
- $|\Delta\eta_{in}| < 0.007/0.009$
- $H/E < 0.12/0.10$ (barrel/endcap)
- $\frac{\sum_{\mathrm{trk}} E_{\mathrm{T}}}{p_{\mathrm{T}}^{\mathrm{ele}}} < 0.2$
- $\frac{\sum_{\mathrm{ECAL}} E_{\mathrm{T}}}{p_{\mathrm{T}}^{\mathrm{ele}}} < 0.2$
- $\frac{\sum_{\mathrm{HCAL}} E_{\mathrm{T}}}{p_{\mathrm{T}}^{\mathrm{ele}}} < 0.2$

Isolation requirements are then imposed by computing the particle flow isolation, defined as the scalar sum of the p_{T} of the particle flow candidates satisfying the following requirements:

- $\Delta R < 0.4$ to the electron in the $\eta \times \phi$ plane,
- for neutral hadron PF candidates, require that it is outside the footprint veto region of $\Delta R < 0.07$,
- for photon and electron PF candidates, require that it is outside the footprint veto region of $|\Delta\eta| < 0.025$,
- $|d_z(\mathrm{PF\ candidate}) - d_z(\mathrm{muon})| < 0.1$ cm, if the PF candidate is charged,
- $p_{\mathrm{T}} > 1.0$ GeV, if the PF candidate is classified as a neutral hadron or a photon.

We require $\frac{\text{Iso}_{\text{PF}}}{p_{\text{T}}} < 0.13$ (0.09) for electrons in the barrel (endcap).

In order to veto fake electrons from converted photons, we look for a reconstructed conversion vertex where one of the two tracks is compatible with the electron [23]. The vertex fit probability is required to be $> 10^{-6}$. We then require that there are no missing expected missing hits forming the electron track [23], [14]. Finally to reduce fake electrons from non-prompt sources, we require the transverse and longitudinal impact parameters with respect to the primary vertex to be less than 0.02 and 0.1 cm respectively.

3.5 Missing Energy

The missing transverse energy is used to reject background events where there is no natural source of missing energy, like in Drell-Yan and QCD events. In the $Z/\gamma^* \to \tau\tau$ process there is a large difference in the masses of τ and Z. The taus are produced with large boost and their decay products, including neutrinos, are aligned with the leptons. Therefore a transverse component of missing energy with respect to the leptons is a better measure of true missing energy in the event, not originating from τ decay. To reject such background events with a small opening angle between $E_{\text{T}}^{\text{miss}}$ and one of the leptons, we used the projected $E_{\text{T}}^{\text{miss}}$ [7] for event selection, defined as:

$$\text{with } \Delta\phi_{min} = min(\Delta\phi(\ell_1, E_{\text{T}}^{\text{miss}}), \Delta\phi(\ell_2, E_{\text{T}}^{\text{miss}})) \tag{1}$$

$$= \begin{cases} E_{\text{T}}^{\text{miss}} & \text{if } \Delta\phi_{min} > \frac{\pi}{2}, \\ E_{\text{T}}^{\text{miss}} \sin(\Delta\phi_{min}) & \text{if } \Delta\phi_{min} < \frac{\pi}{2} \end{cases} \tag{2}$$

where $\Delta\phi(\ell_i, E_{\text{T}}^{\text{miss}})$ is the angle between $E_{\text{T}}^{\text{miss}}$ and lepton i in the transverse plane. In the presence of high multiple-interactions (pile-up), the instrumental $E_{\text{T}}^{\text{miss}}$ tail in $Z/\gamma^* \to \ell\ell$ events increases significantly.

To improve the signal over background performance of $E_{\text{T}}^{\text{miss}}$ selections in the presence of pile-up, we have developed a novel $E_{\text{T}}^{\text{miss}}$ algorithm referred to as "trk-MET" [36], constructed from charged particles consistent with originating from the primary vertex. The event $E_{\text{T}}^{\text{miss}}$ trk-MET is defined as

$$\text{trk-MET} \equiv -\overrightarrow{p_T}(l_1) - \overrightarrow{p_T}(l_2) - \sum_i \overrightarrow{p_T}(i), \tag{3}$$

where $\overrightarrow{p_T}(l_1)$ and $\overrightarrow{p_T}(l_2)$ are the transverse momentum vectors of the two leptons passing the lepton selections described in Section 3.3 and Section 3.4, and $\overrightarrow{p_T}(i)$ represent the tranverse momentum vectors of the charged PFCandidates satisfying the following requirements:

- the track matched to PFCandidate has $\Delta z < 0.1$ cm with respect to the signal primary vertex;
- the track has $\Delta R > 0.1$ with respect to both leptons, to avoid double-counting of the leptons.

Comparing to the projected PFMet, we observed that the projected trk-MET has a larger tail in $Z/\gamma^* \to \ell\ell$ background events [36]. However these two $E_{\text{T}}^{\text{miss}}$ values are weakly-correlated in $Z/\gamma^* \to \ell\ell$ backgrounds with no geninue $E_{\text{T}}^{\text{miss}}$, and strongly correlated for the signal processes with geninue $E_{\text{T}}^{\text{miss}}$. Therefore the signal over background ratio is improved if we select the events based on the mininum of these two projected $E_{\text{T}}^{\text{miss}}$ values, min-MET $\equiv min(\text{proj}_{\text{trk-MET}}, \text{proj}_{\text{PFMET}})$.

The selection requirements are different between $ee/\mu\mu$ and $e\mu$ final states since Drell-Yan mostly contributes to ee and $\mu\mu$ channels. The selection requirements are:

- min-MET > 20 GeV for $e\mu$;
- min-MET $> (37 + N_{vtx}/2)$ GeV for ee and $\mu\mu$.

3.6 *Z* Veto

To further reduce the Drell–Yan background in the e^+e^- and $\mu^+\mu^-$ final states, we veto events with a dilepton invariant mass within 15 GeV of the Z. We also reject events with a dilepton invariant mass below 20 GeV (same-flavor) and 12 GeV (opposite flavor) to suppress contributions from low mass resonances as well as to reject low mass Drell–Yan contribution that is poorly simulated at the moment.

3.7 Jet Veto

Jets are reconstructed using calorimeter and tracker information using a particle flow algorithm [20]. The anti-k_T clustering algorithm [22] with R = 0.5 is used. We apply the standard jet energy corrections [19] to the reconstructed jets, where the L1 Fast Jets corrections are included. The latter corrections are rather important since they help in flatening the reconstruction efficiency as a function of the number of overlapping events. To exclude electrons and muons from the jet sample, these jets are required to be separated from the selected leptons in ΔR by at least $\Delta R^{\mathrm{jet-lepton}} > 0.3$.

In this analysis we veto events with more than zero counted jets. The top tagging is also applied to low p_T jets. We define:

- *counted jet*: a reconstructed jets with $p_{\mathrm{T}} > 30$ GeV within $|\eta| < 5.0$;
- *low p_T jet*: a reconstructed jets with $10 < p_{\mathrm{T}} < 30$ GeV within $|\eta| < 5.0$

3.8 Top Tagging

Because the production cross-section is substantially higher than the W^+W^- cross-section, top backgrounds pose a significant challenge. To reduce the top background, we introduce two top tagging methods. Both methods rely on the fact that top quarks decay to Wb with almost certainty.

The first method vetoes events containing soft muons from the b-quark decays. The requirements used to select soft muons are:

- $p_{\mathrm{T}} > 3$ GeV;
- Reconstructed as a TrackerMuon
- Meets TMLastStationAngTight muon id requirements
- The number of valid inner tracker hits > 10
- The transverse impact parameter with respect to the Primary Vertex, $|d_0| < 0.2$ cm,
- The longitudinal impact parameter with respect to the Primary Vertex $|d_z| < 0.2$ cm. This requirement has been loosened with respect to [7];
- Non-isolated ($\mathrm{Iso}_{\mathrm{Total}}/p_{\mathrm{T}} > 0.1$) if $p_{\mathrm{T}} > 20$GeV.

The second method uses standard b-jet tagging [7]. In this method, events containing jets tagged with the TrkCountingHighEff [21] algorithm with a discriminator value of greater than 2.1 are vetoed. The algorithm is applied to jets with the same definition as Section 3.7, with the exception that we consider jets with $E_{\mathrm{T}} > 10$ GeV, and we require $\frac{|\sum^i d_z^i (p_{\mathrm{T}}^i)^2|}{\sum^i (p_{\mathrm{T}}^i)^2} < 2$, where the sum runs over all tracks that belongs to each jet. These two requirements are different with respect to [7], with the effect of reducing the mistag rate and the dependency on pile-up. By using the expected tagging efficiency for the two methods, it is possible to estimate the residual top background after the vetoes have been applied. This is described in detail in Section 4.2.

3.9 Other Preselection Requirements

To reduce the background from diboson processes, we veto events containing an additional lepton meeting the previously described selection requirements with $p_{\mathrm{T}} > 10$ GeV/c. This removes $\sim 60\%$ of the WZ component and $\sim 10\%$ of the ZZ one. The ZZ component is dominated by ZZ $\to 2l2\nu$ decays. The efficiency for $WW \to 2l2\nu$ events is $\sim 99.9\%$. Finally, the angle in the transverse plane between the dilepton system and the most energetic jet with $p_{\mathrm{T}}^{jet} > 15$ GeV must be smaller than 165 degrees in the $ee/\mu\mu$ final states. This requirements rejects $Z/\gamma^* \to \ell\ell$ events, where the Z boson recoil against a jet.

4 Background Estimation

4.1 Jet Induced Backgrounds

Jet induced fake leptons are an important source of background for many physics channels. In this analysis the main sources of fake leptons are W + jets and QCD events, where at least one of the jets or a constituent is misidentified as an isolated lepton. The dominant background is W + jets because there is already one prompt, well isolated, lepton from the W boson decay. Fake non-prompt leptons arise from the leptonic decay of heavy quarks, misidentified hadrons or electrons from photon conversion.

A data-driven approach, described in detail in [15] and [16], is pursued to estimate this background. Only a summary of the method is described here, more details can be found in [7]. A set of loosely selected lepton-like objects, referred to as the "fakeable object" or "denominator" from here on, is defined in a sample of events dominated by dijet production. The efficiency for these denominator objects to pass the full lepton selection critera is measured. This background efficiency, typically referred to as the "fake rate", is parameterized as a function of the p_{T} and η of the denominator object in order to capture any dependence on kinematic and geometric quantities. We will denote the fake rate symbollically by ϵ_{fake}. These fake rates are, then, used as weights to extrapolate the background yield from a sample of loose denominator objects to the sample of fully selected leptons.

4.1.1 Denominator Object Definitions

The denominator object definition has significant impact on the systematic uncertainty of the method, due to the fact that the sample dependence uncertainties for extrapolating in different isolation and lepton quality criteria are typically different. We consider the following definition:

- $\sigma_{i\eta i\eta} < 0.01/0.03$ (barrel/endcap)
- $|\Delta\phi_{in}| < 0.15/0.10$
- $|\Delta\eta_{in}| < 0.007/0.009$
- $H/E < 0.12/0.10$
- full conversion rejection
- $|d_0| < 0.02$ cm
- $\frac{\sum_{\mathrm{trk}} E_{\mathrm{T}}}{p_{\mathrm{T}}^{\mathrm{ele}}} < 0.2$
- $\frac{\sum_{\mathrm{ECAL}} E_{\mathrm{T}}}{p_{\mathrm{T}}^{\mathrm{ele}}} < 0.2$
- $\frac{\sum_{\mathrm{HCAL}} E_{\mathrm{T}}}{p_{\mathrm{T}}^{\mathrm{ele}}} < 0.2$

The situation for muons is simpler. The loose muon selection requirements can differ from the tight selection of Section 3.3, only in less stringent cuts on d_0 and isolation. We consider the following definition:

- $|d_0| < 0.2$ cm
- $\frac{\mathrm{Iso}_{\mathrm{Total}}}{p_{\mathrm{T}}} < 0.4$

4.1.2 Fake rate measurement

The fake rates are measured in calibration data samples dominated by fake leptons resulting from jets in QCD dijet events. The QCD dijet event sample is collected using a combination of different electron and muon triggers.

In order to suppress contamination due to signal leptons from the decay of W and Z bosons we require that the missing transverse energy is less than 20 GeV, and that the event contains only a single reconstructed lepton. In order to control the average p_T of the jet that fakes the lepton, we impose a p_T requirement on the leading jet in the event and require that the lepton denominator object is separated from the leading

jet by $\Delta R > 1.0$. The nominal fake rates for electrons are measured requiring that the leading jet p_T is greater than 35 GeV, and the nominal fake rates for muons are measured with the requirement that the leading jet p_T is greater than 15 GeV. From these selected event samples, we measure the fake rate (ϵ_{fake}) by counting the number of denominator objects which pass the full lepton selection, in bins of p_T and η.

4.1.3 Application of Fake rates

Having measured the fake rates, parameterized in the kinematic quantities of interest, we then use them as weights in order to extrapolate the yield of the sample of loose leptons to the sample of fully selected leptons. This is done by selecting events passing the full event selection described in Sec.3, with the exception that one of the two lepton candidates is required to pass the denominator selection cuts but fail the full lepton selection cuts. This lepton is from here on denoted the "failing leg". The other lepton is required to pass the full selection. The data sample selected in this way is denoted the "tight + fail" sample. Each of the events passing this selection is given a weight computed from the fake rate in the particular p_T and η bin of the failing leg, as follows:

$$w_i = \frac{\epsilon_{\text{fake}}(p_{\text{Ti}}, \eta_i)}{1 - \epsilon_{\text{fake}}(p_{\text{Ti}}, \eta_i)} \tag{4}$$

where i is an index denoting the failing leg, and p_{Ti} and η_i are the transverse momentum and pseudorapidity of the failing leg. Summing the weights w_i over all such events in the tight + fail sample yields the total jet induced background prediction.

This tight + fail extrapolation prediction will in fact double count the QCD component of the background, where both leptons are jet induced fakes. This is essentially a combinatorial artifact, due to the fact that in the tight plus fail selection, one is unable to uniquely distinguish which lepton is required to be the tight one and which lepton is required to be the failing one, and therefore one customarily selects both combinations. This double fake background is typically very small and accounts for roughly a few percent of the total jet induced background. In order to estimate the amount of double counting, we perform the fake rate extrapolation on both lepton legs, selecting events which pass all event selection criteria, except that both leptons are required to pass the denominator selection, but fail the full lepton selection. This event sample is denoted as the "fail + fail" sample. Events in the fail + fail sample are then given weights as follows:

$$w_{i,j} = \frac{\epsilon_{\text{fake}}(p_{\text{Ti}}, \eta_{\text{i}})}{1 - \epsilon_{\text{fake}}(p_{\text{Ti}}, \eta_{\text{i}})} \times \frac{\epsilon_{\text{fake}}(p_{\text{Tj}}, \eta_{\text{j}})}{1 - \epsilon_{\text{fake}}(p_{\text{Tj}}, \eta_{\text{j}})} \tag{5}$$

where i and j denote the two failing leg, and $p_{\text{Ti/j}}$ and $\eta_{\text{i/j}}$ are the transverse momentum and pseudorapidity of the first and second leg. Summing the weights $w_{i,j}$ over all such events in the fail + fail sample yields the total QCD double fake background. This prediction is then subtracted from the tight + loose prediction in order to account for the double counting.

In this procedure, an over-estimation of the fake lepton contribution due to contamination from real dilepton events, and from $W + \gamma$ events may occur. These contributions are subtracted using the Monte Carlo simulation prediction with the procedure described in [15] and [17].

4.2 Top Background

The top quark induced background in the W^+W^- analysis originates from $t\bar{t}$ and the single top (tW) processes, the latter being especially imporatant in the 0-Jet bin. A consistent theoretical description of the two processes at high perturbation orders is not straightforward to attain as already at NLO some tW diagrams coincides with LO $t\bar{t}$ ones [42]. The Monte Carlo simulated samples used in the analysis exploit an approach recently proposed [43], which addresses the overlap by discarding the common diagrams from the tW process either at amplitude level (*Diagram Removal*) or at cross section level (*Diagram Subtraction*). The former is considered the default scheme, whereas the latter is used as cross check.

The procedure to estimate the top background from data in the case of the 0-Jet bin established in [7] has been adapted to the new theoretical description of $t\bar{t}$ and tW. Before assessing the adjustments to the procedure, it is worth reviewing the key points of the normalization strategy.

Rejection for the top background is achieved by top-tagged events, i.e. events with a b-tagged jet or a soft muon as defined in Section 3.8. The estimation of this background relies on the measurement on data of the top-tagging efficiency. The procedure deployed in [7] in the case of the 0-Jet bin proceeds accordingly to the following steps:

1. A top enriched region is defined requiring exactly one b-tagged jet with p_{T}larger than 30 GeV (denominator). Those events among this sample with at least one b-tagged jets with $10 < p_{\mathrm{T}} < 30$ GeV or one soft muon defines the numerator. The ratio of the yields in the numerator and denominator properly corrected from other backgrounds contamination provides the top-tagging efficiency for one "top-taggable" leg, ϵ_{1leg}^{data}.

2. The actual top-tagging efficiency, ϵ_{topTag}^{data}, is computed accounting for the $t\bar{t}$fraction of the top background ($f_{t\bar{t}}^{MC}$) accordingly to the formula:

$$\epsilon_{topTag}^{data} = f_{t\bar{t}}^{MC}(1-(1-\epsilon_{1leg}^{data})^2) + (1-f_{t\bar{t}}^{MC})\epsilon_{1leg}^{data} \tag{6}$$

   where the first term on the right accounts for $t\bar{t}$ (two taggable legs) and the second term for tW (one taggable leg). The value $f_{t\bar{t}}^{MC}$ is determined from Monte Carlo in the 0-Jet bin at the $\mathrm{W^+W^-}$ preselection level, removing the anti top-tagging.

3. A dedicated control region is defined in the 0-Jet bin by requiring top-tagged events. The data yields in this region corrected for the other backgrounds contaminations are then used together with top-tagging efficiency to predict the top background after $\mathrm{W^+W^-}$ preselections level:

$$N_{WWregion}^{top} = N_{topTag}^{top}\frac{1-\epsilon_{topTag}^{data}}{\epsilon_{topTag}^{data}} = (N_{topTag}^{data} - N_{other-bkg}^{data})\frac{1-\epsilon_{topTag}^{data}}{\epsilon_{topTag}^{data}} \tag{7}$$

In a nutshell, the new procedure refines the way the top-tagging efficiency is extracted from data, taking properly into account the different features of $t\bar{t}$ and tW.

- The top-tagging efficiency for one leg, ϵ_{1leg}^{data}, is computed for $t\bar{t}$ only, that is both non-top backgrounds and tW yields are subtracted from the measured data in the 1-Jet bin control region defined above (both numerator and deniminator). The yields for tW are estimated from the Monte Carlo normalized accordingly to the data-driven predictions in the 1-Jet bin previously evaluated.

- The overall top-tagging efficiency, ϵ_{topTag}^{data}, is then redefined to account for the fraction of tW events that looks like $t\bar{t}$ (x), that is with two top-taggable legs. Equation 6 thus becomes:

$$\epsilon_{topTag}^{data} = (f_{t\bar{t}}^{MC} + x(1-f_{t\bar{t}}^{MC}))(1-(1-\epsilon_{1leg}^{data})^2) + (1-f_{t\bar{t}}^{MC})(1-x)\epsilon_{1leg}^{data} \tag{8}$$

  The fraction x matches the value of ϵ_{1leg} estimated from the tW Monte Carlo. We consider this a good approximation as ϵ_{1leg} is the fraction of events with one b-tagged jet with p_{T}larger than 30 GeV (the first "top-taggable" leg) and top-tagged leg (a b-tagged jets below 30 GeV or a soft muon).

The extrapolation from the top background control region in the 0-Jet bin to the signal $\mathrm{W^+W^-}$ region is still performed accordingly to Equation 7, where ϵ_{topTag}^{data} is now defined by Eq. 8.

The plots in Figure 1 show the distribution of the b-tag discrimiator for the jet with p_{T} lower than 30 GeV and the highest b-tag discriminator in the denominator and numerator of the control region.

4.3 Drell-Yan Background

We apply a data-driven method [18] to estimate the $Z/\gamma^* \to \ell\ell$ contributions in the same flavor $\ell^+\ell^-$ final states. The expected contributions from $Z/\gamma^* \to \ell\ell$ events outside the Z-mass region in data can be estimated by counting the number of events near the Z mass region in data, subtracting from it

Parameter	Value
Estimated top events in simulation	91.5 ± 1.7
tagging efficiency (%)	51.3 ± 4.1
top-tagged events in data	165
background events in control region	33.0 ± 13.4
Data-driven top background estimate	125.3 ± 24.4
Scale factors	1.37 ± 0.27

Table 3: Monte Carlo to data scale factor for the top background contribution for 4.63 fb^{-1}.

the non-Z contributions, and scaling it by a ratio $R_{out/in}$ defined as the fraction of events outside and inside the Z-mass region in the simulation. The Z-mass region is selected to be within 7.5 GeV of the nominal Z mass. The tight window is chosen to reduce the non-Z contributions from top and multi-boson backgrounds. The non-Z contributions close to the Z-mass region in data is estimated from the number of events in the $e^{\pm}\mu^{\mp}$ final state $N_{in}^{e\mu}$, applying a correction factor that normalizes the electron-to-muon efficiency $k_{ee/\mu\mu}$. $R_{out/in}$ can be obtained both from simulation and data. In simulation it is defined as the ratio N_{out}^{MC}/N_{in}^{MC}.

This method is described mathematically as:

$$N_{out}^{ll,exp} = R_{out/in}^{ll}(N_{in}^{ll} - 0.5N_{in}^{e\mu}k_{ll}), \tag{9}$$

where $k_{ee} = \sqrt{\frac{N_{in}^{ee,loose}}{N_{in}^{\mu\mu,loose}}}$ for $Z/\gamma^* \to ee$ and $k_{mm} = \sqrt{\frac{N_{in}^{\mu\mu,loose}}{N_{in}^{ee,loose}}}$ for $Z/\gamma^* \to \mu\mu$. In the k_{ll} calcualtion, we apply a loose $E_{\mathrm{T}}^{\mathrm{miss}}$ cut on minMET of 20 GeV.

The ZZ/ZW processes contribute to the events in the control region of the $m_{\ell\ell}$ region dominated by the DY. The contribution from ZZ/ZW becomes comparable to the Drell-Yan background after a tight projected $E_{\mathrm{T}}^{\mathrm{miss}}$selection in the same flavor final states. The ZZ/ZW events contain natural $E_{\mathrm{T}}^{\mathrm{miss}}$, for which the detector simulation is reliable[1)]. We subtract the expected peaking ZZ/ZW contribution to the yield in the Z peak using the simulation in the estimation of number of events within the Z window in data:

$$N(\ell\ell)_{\mathrm{signal}}^{\mathrm{DY}} = (N(\ell\ell)_{\mathrm{control}}^{\mathrm{data}} - 0.5 \times N(e\mu)_{\mathrm{control}}^{\mathrm{data}} \times k_{\ell\ell} - N_{\mathrm{control}}^{\mathrm{ZV,\ sim.}}) \times R(\ell\ell)_{out/in}^{DY} \tag{10}$$

The ZZ/ZW contribution in the same flavor final states is then taken directly from simulation. Seperating the Drell-Yan and ZZ/WZ components accounts for the fact that the extrapolation from control region to signal region can be different for the two processes when considering the full Higgs selection. We

[1)] The ZZ/ZW events with no $E_{\mathrm{T}}^{\mathrm{miss}}$are suppressed by the same large factor as the DY ones, and therefore their contribution is as negligible at the level of the final selection as it would be in the yield at the Z peak without $E_{\mathrm{T}}^{\mathrm{miss}}$requirement.

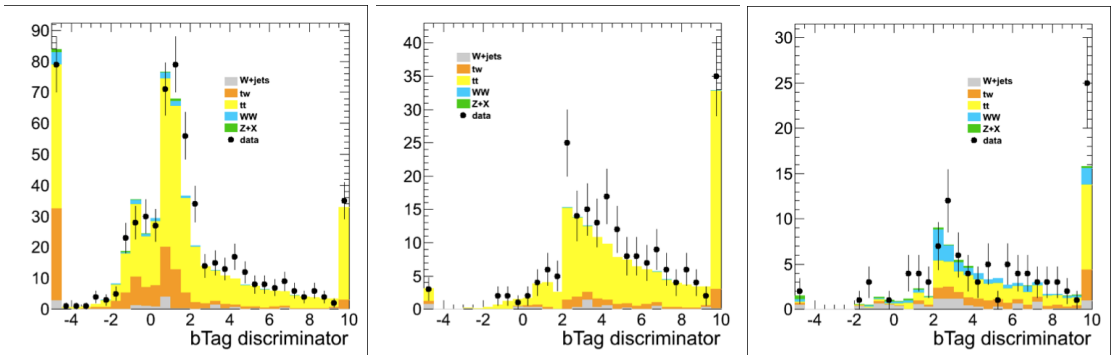

Figure 1: b-tag discrimiator distribution for the jet with $p_T < 30$ GeV and the highest b-tag discriminator in the 1-Jet (denominator, left and numerator, center) and 0-Jet bins control region (right).

Final State	$N(\ell\ell)^{\rm data}_{\rm control}$	$N^{\rm ZV,\ sim.}_{\rm control}$	$R_{out/in}$	N_{out} (data)
ee	108	$48.3 \pm 0.7 \pm 4.8$	$0.12 \pm 0.02 \pm 0.06$	$7.7 \pm 2.5 \pm 3.3$
$\mu\mu$	151	$69.5 \pm 0.8 \pm 7.0$	$0.15 \pm 0.02 \pm 0.07$	$4.9 \pm 1.6 \pm 2.4$
$e\mu$	48	-	-	-
ee and $\mu\mu$ combined	259	$117.8 \pm 1.0 \pm 11.8$	$0.14 \pm 0.02 \pm 0.06$	$12.7 \pm 3.3 \pm 5.4$

Table 4: Predictions of the off-peak Z/γ^* contribution for events passing all WW selections. Both statistical and systematic uncertainties are displayed. For the VZ contribution in the control region, we assign 10% systematics due to the uncertainty in the cross-sections.

assume an overall 10% uncertainty on the ZZ/ZW yield in the peak, which is anyway overshadowed by the statistical uncertainty on the observed events in the Z peak in data.

This $Z/\gamma^* \to \ell\ell$ estimation method relies on the assumption that the dependence of the ratio $R_{out/in}$ on the $E_{\rm T}^{\rm miss}$ cut is well modelled by simulation and is relatively flat. The variations in the $R_{out/in}$ in different $E_{\rm T}^{\rm miss}$ regions are assigned as systematics. The $E_{\rm T}^{\rm miss}$ regions considered are [20, 23], [23-28], [28-37] and [37, above]. As we do not see any statistically difference between the ee and $\mu\mu$ final states, we combine the two final states to gain statistical stability.

We cross-checked the $R_{out/in}$ value in data as well. Background processes contribute equally to ee, $e\mu$, μe and $\mu\mu$ final states (after efficiency corrections), while Drell-Yan only contributes to ee and $\mu\mu$. Therefore we can subtract $e\mu$ and μe contribtutions from ee and $\mu\mu$ ones to get an estimate of Drell-Yan. We have found good agreement between data and MC in the Drell-Yan dominated regions, shown in Figure 2. We do not observe a trend in the dependence of R with the $E_{\rm T}^{\rm miss}$ cuts. For the final estimate, we choose the R value obtained in the $E_{\rm T}^{\rm miss}$ regions of [28-37] GeV which contains more statistics then the signal region. The largest difference of R in other $E_{\rm T}^{\rm miss}$ regions from the nominal value is assigned as the systematic error.

Table 4 shows the results of Drell-Yan background estimation for the 4.63 fb^{-1} data.

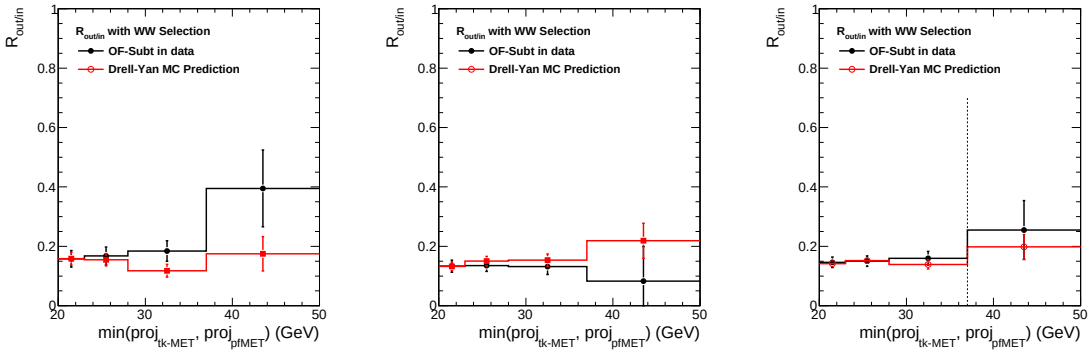

(a) ee (b) mm (c) ee/mm combined

Figure 2: The $R_{out/in}$ as a function of MET measured from data (black solid dots) and MC (red open circles) for the Drell-Yan processes. The measurements in data are done using the opposite flavor subtraction method.

4.4 Other Backgrounds

The WZ and ZZ events with lepton pairs from a resonant Z boson are suppressed by the Z veto. The remaining contribution is estimated from simulation, after applying the proper data to simulation correction factors for the lepton and trigger efficiencies.

The $W + \gamma$ background, where the γ fakes an electron through an asymmetric conversion is difficult to estimate from data. Additional cross-checks can be performed to place data based constraints on this estimate. For instance, applying the same standard selection, but requiring two same-sign leptons, gives

a sample dominated by W + jets and $W + \gamma$ events. Again, the expected contribution is very small, due to stringent γ conversion requirements explained in Sec. 3.4.

The electroweak process Wγ^* enters the signal region if one of the leptons from the γ^* is lost. This background is normally covered in Monte Carlo simulations as a part of the WZ process. However in the simulation, there is a generator level cut of $m_{\gamma^*} > 12$ GeV, and there is a significant rate of events at lower values [44]. A dedicated $W\gamma^*$ sample is simulated in Madgraph with $m_{\gamma^*} < 12$ GeV. The prediction from this simulation is then normalized to data according to the rate in the $W\gamma^*$ enriched region, as detailed in Ref. [8]. The normalization factor applied is 1.53.

The $Z/\gamma^* \to \tau\tau$ background is suppressed signficiantly by the projected $E_{\mathrm{T}}^{\mathrm{miss}}$ requirements as the $E_{\mathrm{T}}^{\mathrm{miss}}$ tend to be aligned with one of the leptons. However the large amount of pileup interactions may lead to fake $E_{\mathrm{T}}^{\mathrm{miss}}$ that is larger than the natural $E_{\mathrm{T}}^{\mathrm{miss}}$ in $Z/\gamma^* \to \tau\tau$ events. Given that the fake $E_{\mathrm{T}}^{\mathrm{miss}}$ can not be reliably estimated in simulation, we developped two data-driven methods to estimate the $Z/\gamma^* \to \tau\tau$ background as documented in Ref. [8]. Both methods find that the $Z/\gamma^* \to \tau\tau$ rate in data is a factor of 4 larger than the value predicted by simulation.

5 Efficiency Measurements

5.1 Lepton Efficiency

We used the tag and probe method on $Z/\gamma^* \to \ell\ell$ events to provide an unbiased, high-purity, lepton sample with which to measure both online and offline selection efficiencies. This method, which is now described, has been used successfully in previous CMS analyses [31][32].

5.1.1 Method

For muons, we used the lowest threshold unprescaled single muon triggered sample from the Prompt Reco. For electrons we used events triggered by the dedicated double electron tag and probe trigger, where tight electron requirements are imposed on one leg and the other leg is a super cluster.

At least one of the leptons, the *tag*, was required to pass the full selection criteria while the other lepton, the *probe*, was required to pass a set of identification criteria leaving it unbiased with respect to the criterion under study. By requiring that the tag was able to have passed the single lepton trigger on which the events were acquired, we reduced the bias due to the trigger on the probe. Also, the tight criteria imposed on the tag coupled with the invariant mass requirement improves the purity of the sample. Because the analysis uses the same mass window to reduce the $Z/\gamma^* \to \ell\ell$ contribution, the tag and probe sample represents an independent control sample. The method used is identical to that in Ref. [8], where more details can be found.

The offline selection results shown here use the N-1 method with simple counting. We split the results into the detector regions $|\eta| < 1.479$ and $1.479 < |\eta| < 2.50$ to reflect the divisions that define our event selections. The trigger selection results are shown in the minimum number of bins required to capture the efficiency below the kinematic turn-on, in the region of the turn-on and at plateau.

To produce overall data-MC scale factors to apply in the analysis, we factorise the efficiency measurements into two steps such that

$$\varepsilon_{total} = \varepsilon_{offline} \times \varepsilon_{trigger}. \tag{11}$$

The offline efficiency $\varepsilon_{offline} = \varepsilon^{l1}_{offline} \times \varepsilon^{l2}_{offline}$ is the product of the efficiencies of the two leptons and is discussed in more detail in Sections 5.1.2 and 5.1.3 for electrons and muons respectively. The trigger efficiency is measured with respect to the offline selection and is discussed in more detail in Section 5.1.4.

5.1.2 Electron Efficiency

The electron selection efficiency can be factorised into two contributions, the efficiency from the electron reconstruction and from the additional analysis selections that are described in Section 3.4.

The electron reconstruction efficiency is defined as the efficiency for a supercluster to be matched to a reconstructed ECAL driven GSF electron. The data to simulation scale factor was measure by the

Egamma POG binned in p_T and η [33]. From these studies, we take an overall scale factor of 0.99 with an uncertainty of 1.0%.

We thus measure the efficiency of our offline analysis selection with respect to a reconstructed ECAL driven GSF electron denominator. For electrons with p_T above 20 GeV the efficiency is roughly 80% for the barrel and 65% for the endcap. The Monte Carlo to data scale factors for the electron selection efficiency are on average near 1 for all electrons except endcap electrons with p_T below 20 GeV for which the scale factor is roughly 1.1.

The electron efficiencies measured in Monte Carlo simulation and data as well as the scale factor are shown in Table 5 for the 2011A, 2011B and full 2011 data. Further details can be found in Ref. [8].

p_T / η bin	Monte Carlo Efficiency	Data Efficiency	MC to Data Scale Factor
Run2011A dataset.			
$20.0 < p_T$, $0.0 \leq \lvert\eta\rvert < 1.479$	0.8366 +/- 0.0001	0.8291 +/- 0.0007	0.9910 +/- 0.0009
$20.0 < p_T$, $1.479 \leq \lvert\eta\rvert < 2.5$	0.6498 +/- 0.0003	0.6700 +/- 0.0002	1.0310 +/- 0.0005
Run2011B dataset.			
$20.0 < p_T$, $0.0 \leq \lvert\eta\rvert < 1.479$	0.8249 +/- 0.0001	0.8118 +/- 0.0004	0.9840 +/- 0.0005
$20.0 < p_T$, $1.479 \leq \lvert\eta\rvert < 2.5$	0.6103 +/- 0.0003	0.6271 +/- 0.0016	1.0274 +/- 0.0026
Full 2011 dataset.			
$20.0 < p_T$, $0.0 \leq \lvert\eta\rvert < 1.479$	0.8305 +/- 0.0001	0.8225 +/- 0.0002	0.9904 +/- 0.0003
$20.0 < p_T$, $1.479 \leq \lvert\eta\rvert < 2.5$	0.6292 +/- 0.0003	0.6536 +/- 0.0001	1.0388 +/- 0.0005

Table 5: Offline electron selection efficiencies.

5.1.3 Muon Efficiency

The muon selection efficiency and the resulting data to simulation scale factors are estimated using a similar method to the electron efficiency. The efficiency for reconstructing a global muon or a tracker muon with respect to a track is measured to be consistent with 100% for the Run2011A period, while it is roughly 99% in the region of the detector covered by the CSC muon detectors in the Run2011B period.

We measure the offline muon selection efficiency with respect to a reconstructed global muon or tracker muon denominator. The Monte Carlo to data scale factors for the muon selection efficiency are on average around 0.97 for p_T below 20 GeV and 0.99 for p_T above 20 GeV. Analogous to electrons, there is a decrease in signal muon efficiency of $7-8$% from the Run2011A period to the Run2011B period for muons with p_T below 20 GeV, and a corresponding but smaller decrease in the Monte Carlo to data scale factor.

The muon efficiencies measured in Monte Carlo simulation and data as well as the scale factor are shown in Table 6 for the 2011A, 2011B and full 2011 data. Further details can be found in Ref. [8].

p_T / η bin	Monte Carlo Efficiency	Data Efficiency	MC to Data Scale Factor
Run2011A dataset.			
$20.0 < p_T$, $0.0 \leq \lvert\eta\rvert < 1.5$	0.9996 +/- 0.0000	0.9988 +/- 0.0000	0.9992 +/- 0.0000
$20.0 < p_T$, $1.5 \leq \lvert\eta\rvert < 2.4$	0.9996 +/- 0.0000	0.9935 +/- 0.0002	0.9939 +/- 0.0002
Run2011B dataset.			
$20.0 < p_T$, $0.0 \leq \lvert\eta\rvert < 1.5$	0.9552 +/- 0.0001	0.9483 +/- 0.0002	0.9928 +/- 0.0002
$20.0 < p_T$, $1.5 \leq \lvert\eta\rvert < 2.4$	0.9145 +/- 0.0001	0.9116 +/- 0.0005	0.9969 +/- 0.0005
Full 2011 dataset.			
$20.0 < p_T$, $0.0 \leq \lvert\eta\rvert < 1.5$	0.9525 +/- 0.0001	0.9447 +/- 0.0002	0.9918 +/- 0.0002
$20.0 < p_T$, $1.5 \leq \lvert\eta\rvert < 2.4$	0.9064 +/- 0.0002	0.8915 +/- 0.0001	0.9835 +/- 0.0002

Table 6: Offline muon selection efficiencies.

5.1.4 Trigger Efficiency

To determine the efficiency of the dilepton triggers, we derive the efficiency of the requirements imposed on each leg separately. This requires a modification to the tag and probe method described above in some cases. If the trigger objects are saved by the HLT before the requirement that there be two valid objects then we can check each leg independently of the other using the usual tag and probe method. If the trigger objects are saved after the requirement that there are two valid objects, then there is a 100% correlation between the decision we can probe on each lepton. This means that we must pick exactly one tag candidate for each event a priori, which we do randomly. If the randomly selected tag candidate meets the tight requirements then we are free to probe the other lepton.

The double electron trigger requires the higher p_T leg to be seeded at Level-1. The efficiency of the seeded and unseeded legs with respect to an electron passing offline selection is tabulated in Table 7. The efficiency of the single electron trigger with respect to an electron passing offline selection is given in Table 8. The listed values represent the overall efficiencies averaged over the run range of the dataset, absorbing changes in thresholds and seeding requirements over time. The efficiency of the leading and trailing legs of the double muon trigger is summarized in Table 9. The efficiency of the single muon trigger is given in Table 10.

In the case of the $e\mu$ triggers, we cross check the trigger efficiency against the leading and trailing legs of the double electron and double muon triggers using dilepton $t\bar{t}$ events requiring that the event has missing transverse energy greater than 20 GeV. The efficiency of the muon leg are measured using events passing the single electron trigger, while the efficiency of the electron leg are measured using events passing the single muon trigger. They are found to be consistent within statistical uncertainties. We thus take the single leg efficiencies from the double electron and double muon triggers for the cross triggers as well.

Measurement	$0.0 \leq \lvert\eta\rvert < 1.5$	$1.5 \leq \lvert\eta\rvert < 2.5$
Leading leg requirement.		
$20.0 < p_T \leq 30.0$	0.9849 +/- 0.0003	0.9774 +/- 0.0007
$30.0 < p_T$	0.9928 +/- 0.0001	0.9938 +/- 0.0001
Trailing leg requirement.		
$20.0 < p_T \leq 30.0$	0.9923 +/- 0.0002	0.9953 +/- 0.0003
$30.0 < p_T$	0.9948 +/- 0.0001	0.9956 +/- 0.0001

Table 7: The per leg efficiency of the double electron trigger, averaged over the full 2011 dataset.

Measurement	$0.0 \leq \lvert\eta\rvert < 1.5$	$1.5 \leq \lvert\eta\rvert < 2.5$
$20.0 < p_T \leq 25.0$	0.0002 +/- 0.0001	0.0001 +/- 0.0002
$25.0 < p_T \leq 30.0$	0.0314 +/- 0.0006	0.0144 +/- 0.0007
$30.0 < p_T \leq 35.0$	0.1511 +/- 0.0009	0.1303 +/- 0.0016
$35.0 < p_T \leq 40.0$	0.2318 +/- 0.0008	0.2496 +/- 0.0017
$40.0 < p_T \leq 50.0$	0.2342 +/- 0.0006	0.2327 +/- 0.0011
$50.0 < p_T \leq 65.0$	0.2899 +/- 0.0013	0.2502 +/- 0.0022
$65.0 < p_T \leq 80.0$	0.8170 +/- 0.0027	0.5012 +/- 0.0065
$80.0 < p_T$	0.9470 +/- 0.0020	0.9193 +/- 0.0048

Table 8: The efficiency of the single electron trigger, averaged over the full 2011 dataset.

Having measured the per lepton trigger efficiencies and for the double and single trigger, we compute the efficiency for dilepton events to be selected. We do this by taking into account the two ways an event can be selected: the double trigger can pass or the double trigger can fail because one leg is bad but the good leg can pass the single trigger. If both legs are bad in the double trigger they will also both be bad in the single trigger because the requirements of the single trigger are tighter than any single leg of the double trigger. Thus taking into account combinatorics, the event efficiency $\varepsilon_{\ell\ell'}(p_T,\, \eta,\, p'_T,\, \eta')$ is given in Equation 12, where $\varepsilon_S(p_T,\, \eta)$ is the single lepton trigger efficiency, $\varepsilon_{\mathrm{D,leading}}(p_T,\, \eta)$ is the efficiency of the leading leg of the appropriate double trigger, and $\varepsilon_{\mathrm{D,trailing}}(p_T,\, \eta)$ is the efficiency of the trailing leg of the appropriate double trigger.

Measurement	$0.0 \leq \|\eta\| < 0.8$	$0.8 \leq \|\eta\| < 1.2$	$1.2 \leq \|\eta\| < 2.1$	$2.1 \leq \|\eta\| < 2.4$
Leading leg requirement.				
$20.0 < p_T \leq 30.0$	0.9648 +/- 0.0007	0.9516 +/- 0.0013	0.9480 +/- 0.0009	0.8757 +/- 0.0026
$30.0 < p_T$	0.9666 +/- 0.0003	0.9521 +/- 0.0005	0.9485 +/- 0.0004	0.8772 +/- 0.0012
Trailing leg requirement.				
$20.0 < p_T \leq 30.0$	0.9655 +/- 0.0007	0.9535 +/- 0.0013	0.9558 +/- 0.0009	0.9031 +/- 0.0023
$30.0 < p_T$	0.9670 +/- 0.0003	0.9537 +/- 0.0005	0.9530 +/- 0.0004	0.8992 +/- 0.0011

Table 9: The per leg efficiency of the double muon trigger, averaged over the full 2011 dataset.

Measurement	$0.0 \leq \|\eta\| < 0.8$	$0.8 \leq \|\eta\| < 1.5$	$1.5 \leq \|\eta\| < 2.1$	$2.1 \leq \|\eta\| < 2.4$
$15.0 < p_T \leq 24.0$	0.2799 +/- 0.0022	0.2723 +/- 0.0023	0.2706 +/- 0.0024	0.2264 +/- 0.0034
$24.0 < p_T \leq 30.0$	0.4659 +/- 0.0016	0.4449 +/- 0.0019	0.4549 +/- 0.0021	0.3294 +/- 0.0030
$30.0 < p_T \leq 40.0$	0.9002 +/- 0.0005	0.8352 +/- 0.0008	0.8266 +/- 0.0009	0.3345 +/- 0.0019
$40.0 < p_T$	0.9440 +/- 0.0003	0.8821 +/- 0.0005	0.8611 +/- 0.0007	0.3453 +/- 0.0017

Table 10: The efficiency of the single muon trigger, averaged over the full 2011 dataset.

$$
\begin{aligned}
\varepsilon_{\ell\ell'}(p_T,\, \eta,\, p'_T,\, \eta') \;=\;& 1 - [(1 - \varepsilon_{\mathrm{D,leading}}(p_T,\, \eta))(1 - \varepsilon_{\mathrm{D,leading}}(p'_T,\, \eta')) && (12)\\
&+ \varepsilon_{\mathrm{D,leading}}(p_T,\, \eta)(1 - \varepsilon_{\mathrm{D,trailing}}(p'_T,\, \eta')) && (13)\\
&+ \varepsilon_{\mathrm{D,leading}}(p'_T,\, \eta')(1 - \varepsilon_{\mathrm{D,trailing}}(p_T,\, \eta))] && (14)\\
&+ \varepsilon_S(p'_T,\, \eta')(1 - \varepsilon_{\mathrm{D,trailing}}(p_T,\, \eta)) \\
&+ \varepsilon_S(p_T,\, \eta)(1 - \varepsilon_{\mathrm{D,trailing}}(p'_T,\, \eta')) && (15)
\end{aligned}
$$

The procedure of Equation 12 is applied to simulated $\mathrm{W^+W^-}$ decays to obtain an event-by-event weight factor. We find a trigger efficiency with respect to the offline selection of 98% for both the $qq \to \mathrm{W^+W^-}$ and $qq \to \mathrm{W^+W^-}$ processes.

5.2 Jet Veto Efficiency

We apply a data-driven method to estimate the jet veto efficiency and its systematic uncertainties in data. In this method, the jet veto efficiency on $\mathrm{W^+W^-}$ events in data $\epsilon_{\mathrm{W^+W^-}}$ is estimated to be the value obtained from simulation multiplied by a data to simulation scale factor from $Z/\gamma^* \to \ell\ell$ events such that,

$$\epsilon_{WW} = \epsilon_{WW}^{MC}(\tfrac{\epsilon_Z^{data}}{\epsilon_Z^{MC}})$$

The jet veto efficiency uncertainty of WW can be factorized into the Z efficiency uncertainty in data and WW/Z efficiency ratio uncertainty in simulation. The former is statistically dominated, while theoretical uncertainties due to higher order corrections contribute most to the WW/Z efficiency ratio uncertainties.

The $Z/\gamma^* \to \ell\ell$ jet veto efficiencies are measured in data and compared with the values obtained from Powheg and Madgraph simulations. Fig. 3 shows the dependence of the $Z/\gamma^* \to \ell\ell$ jet veto efficiency on the jet p_T, comparing data and simulations. The results for jet veto efficiency with the thresold of 30 GeV are summarized in Tab. 11. The data over simulation correction factor is found to be consistent with unity in both ee and $\mu\mu$ final states.

The theoretical uncertainties on the WW/Z jet veto efficiency is evaluated by assessing the impact by the scale variations in both MCFM and MC@NLO. The uncertainty is quantified as the maximum change induced varying the renormalization and factorization scales independently. Details are given in Ref. [48]. The relative systematic uncertainty is found to be 4.6%.

samples	all vtx bins	nVtx <= 5	5 < nVtx < 10	nVtx >= 10
ee Final State				
data	0.83 ± 0.00	0.84 ± 0.00	0.83 ± 0.00	0.81 ± 0.00
powheg MC	0.83 ± 0.00	0.85 ± 0.00	0.83 ± 0.00	0.80 ± 0.00
madgraph MC	0.82 ± 0.00	0.84 ± 0.00	0.82 ± 0.00	0.79 ± 0.00
data/powheg MC	1.00 ± 0.00	0.99 ± 0.00	1.00 ± 0.00	1.01 ± 0.00
data/madgraph MC	1.01 ± 0.00	1.00 ± 0.00	1.01 ± 0.00	1.03 ± 0.00
$\mu\mu$ Final State				
data	0.83 ± 0.00	0.85 ± 0.00	0.84 ± 0.00	0.82 ± 0.00
powheg MC	0.84 ± 0.00	0.85 ± 0.00	0.84 ± 0.00	0.81 ± 0.00
madgraph MC	0.82 ± 0.00	0.84 ± 0.00	0.83 ± 0.00	0.79 ± 0.00
data/powheg MC	1.00 ± 0.00	0.99 ± 0.00	0.99 ± 0.00	1.01 ± 0.00
data/madgraph MC	1.01 ± 0.00	1.01 ± 0.00	1.01 ± 0.00	1.03 ± 0.00

Table 11: The jet veto efficiency and its data/simulation ratios on Z events, using particle flow jets with the corrections described in Section 3.7. The jet veto thresold is 30 GeV.

6 Systematic Uncertainties

FIXME: Table 12 values to be confirmed still appropriate for WW.

We have taken into account the following systematic uncertainties:

- *Luminosity:* We assume an uncertainty of 4.5% since at this moment there are some concerns about the actual luminosity measurements at CMS.
- *Lepton identification and trigger efficiencies:* We measure the efficiencies in data using the tag and probe method that is described in detail in Section 5.1. The estimated uncertainty is about 2% per lepton leg.
- *Momentum scale:* Due to several factors, the energy scale for electrons and the momentum scale for muons have relatively large uncertainties in the current data processing. We assign a systematic uncertainty by varying the transverse momentum of the muons by 1%, and 2% and 5% for electrons

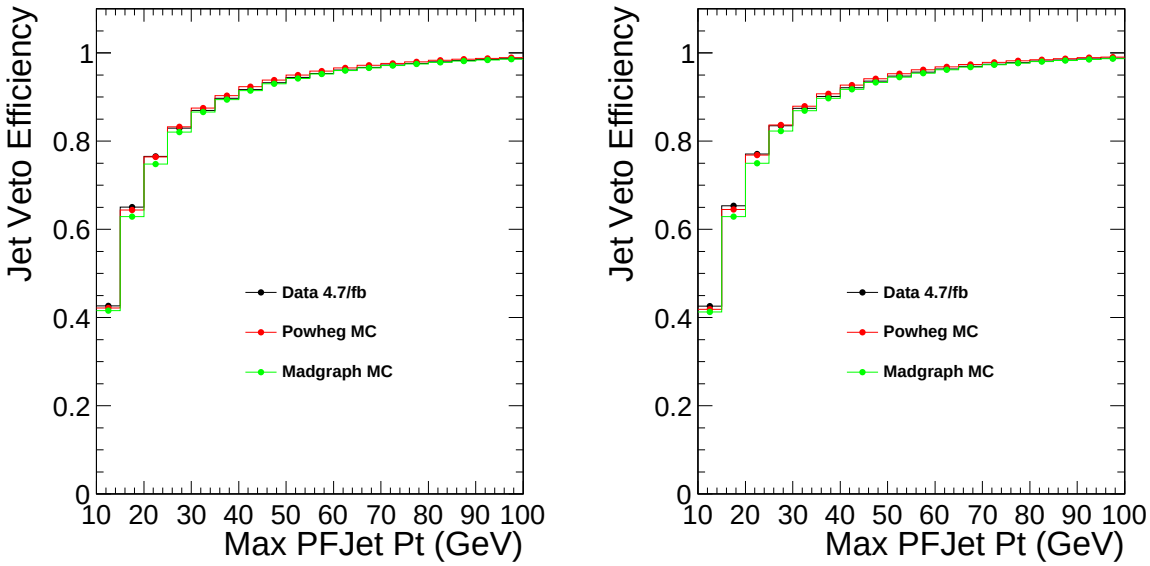

Figure 3: Jet veto efficiency of $Z/\gamma^* \to ee$ (left) and $Z/\gamma^* \to \mu\mu$ (right) events, comparing data with Powheg and Madgraph simulations.

in the barrel and the endcap, respectively. The contribution to the uncertainty on the dilepton efficiency is about 1.5%.

- $E_{\mathrm{T}}^{\mathrm{miss}}$ *modeling:* We use a data-driven method to estimate the $Z/\gamma^* \to \ell\ell$ background, which is affected by the $E_{\mathrm{T}}^{\mathrm{miss}}$ resolution. Events with neutrinos giving real $E_{\mathrm{T}}^{\mathrm{miss}}$ in the final state also have a small uncertainty. We assess this uncertainty on the event selection efficiency by varying the $E_{\mathrm{T}}^{\mathrm{miss}}$ in signal events by an additional 10%. We find an uncertainty on the event selection efficiency of around 2%.

- *Background estimation:* The methods to estimate the different backgrounds are explained in Section 4. Here we summarize the systematic uncertainties associated with the methods used.

  - Jet induced backgrounds, W + jets and QCD: the associated systematic uncertainty is 36%.
  - Top background: this background is estimated using b-tagged events and the b-tagging efficiency, which is measured in control regions in data. The associated systematic uncertainties are below 5%, while the statistical component is about 25% for 4.63 fb^{-1}.
  - Drell-Yan background: The uncertainty arises from the limited knowledge of events with large $E_{\mathrm{T}}^{\mathrm{miss}}$ tails. We conservatively quantify such uncertainty from the variation of the ratio $R_{out/in}$ (Eq.9) as a function of the $E_{\mathrm{T}}^{\mathrm{miss}}$ requirement, leading to an estimate of about 43%.
  - Other backgrounds: The sub-dominant backgrounds are estimated from simulation with appropriate systematic uncertainties on their cross section. The theoretical uncertainties on the WZ and ZZ are estimated the same way as in the signal detailed in below. These uncertainties must be augmented by the luminosity normalization uncertainty.

- *Pileup:* an incorrect modeling of the pileup in the Monte Carlo samples can bias the expected event yields. The simulated events have been re-weighted on the basis of the number of reconstructed primary vertices. The re-weighting procedure affects only slightly the results of the analysis, the event yields changing by $\sim$ 1%. Ongoing investigations considering different pileup models in Summer11 and Fall11 simulation we find a $\sim$ 2.3% effect. Thus we currently assume the latter as a conservative systematic uncertainty.

- *Jet veto efficiency:* This is dominated by the theoretical uncertainty, and is found to be 4.6%. We add in quardrature another 1% coming from the difference of jet veto efficiency measured in data from simulation.

- *Theoretical uncertainties:*

  We evalute the theoretical uncertainties due to the uncertainties in the PDFs and QCD high order effects to the selection efficiency and normalizations for the WW signal and the backgrounds that are evaluated from MC (WZ and ZZ).

  In order to assign systematic uncertainties due to PDFs, we follow the strategy defined by the CMS Generator Group described in [25], which is consistent with the latest PDF4LHC recommendations [26]. The 68% CL of the positive and negative uncertainties obtained with CTEQ66 [27], MSTW2008NLO [28] and NNPDF2.0 [29] sets are considered, adopting the specific recommended recipes in each case. The final assigned systematic uncertainties corresponds to half of the maximum difference observed between positive and negative variations for any combination of the three sets. The maximum difference corresponds to a positive variation from one set minus a negative variation from a different set, since central values from different sets are typically of the size of the uncertainties within a set. Uncertainties due to α_s are also considered. An uncertainty of about 2.3% has been estimated for the signal.

  We have also computed the change of the acceptance of having two lepton in the fiducial region when varying renormalization and factorization QCD scales. The test serves to estimate the accuracy of the cross-section via the stability of the perturbative expansion. In this course it is common to vary the renormalization and factorization scales around some default scale choice, which is usually chosen to be at the order of the scale of the hard-scattering process. For each process we thus define some default scale μ_0, which is the mass of the boson or particle under study, and vary in the range $\mu_0/2 < \mu_F = \mu_R < 2 \times \mu_0$. We find an uncertainty due to the change on the kinematical requirements of about 1.5% percent due these effects to the WW signal.

- *Monte Carlo statistics:* We also take into account the size of the simulated event samples.

Table 12: Summary of all systematic uncertainties (relative).

Source	$qq \to$ $\mathrm{W^+W^-}$	$gg \to$ $\mathrm{W^+W^-}$	WZ	ZZ	top	$Z/\gamma^* \to \ell\ell$	W + jets	$W + \gamma$	$W + \gamma*$	$Z/\gamma^* \to \tau\tau$
Luminosity	4.5	4.5	4.5	4.5	—	—	—	—	4.5	—
Trigger efficiencies	1.5	1.5	1.5	1.5	—	—	—	—	1.5	—
Muon efficiency	1.5	1.5	1.5	1.5	—	—	—	—	1.5	—
Electron id efficiency	2.0	2.0	2.0	2.0	—	—	—	—	2.0	—
Momentum scale	1.5	1.5	1.5	1.5	—	—	—	—	1.5	—
$E_{\mathrm{T}}^{\mathrm{miss}}$ resolution	2.0	2.0	2.0	2.0	—	—	—	—	2.0	—
Jet veto	4.7	4.7	4.7	4.7	—	—	—	—	4.7	—
PDF uncertainties	1.3	0.8	6.5	4.8	—	—	—	—	4.8	—
QCD scale uncertainties	1.5	30	4.2	1.8	—	—	—	—	1.8	—
Pile up	2.3	2.3	2.3	2.3	—	—	—	—	2.3	—
W + jets norm.	—	—	—	—	—	—	36	—	—	—
top norm.	—	—	—	—	19	—	—	—	—	—
$Z/\gamma^* \to \ell\ell$ norm.	—	—	—	—	—	43	—	—	—	—
$Z/\gamma^* \to \tau\tau$ norm.	—	—	—	—	—	—	—	—	—	10
$W + \gamma$ cross section	—	—	—	—	—	—	—	30	—	—
$W + \gamma*$ cross section	—	—	—	—	—	—	—	—	30	—

7 Cross Section Measurement

We now calculate the W^+W^- production cross section according to equation 16,

$$\sigma_{WW} = \frac{N_{data} - N_{bkg}}{\epsilon \cdot \mathcal{L} \cdot BR(WW \to \ell\nu\ell\nu)} \tag{16}$$

Where N_{data} is the number of events observed in data, N_{bkg} is the estimated number of background events, which are summarised with their uncertainties in Table 13. The efficiency to select $\sigma_{WW\to 2\ell 2\nu}$ candidates, ε, is computed as the weighted mean of the $qq \to W^+W^-$ and $gg \to W^+W^-$ efficiencies in simulation. Assuming a 3% contribution from the gg process, ε is found to be $(3.412 \pm 0.235)\%$. The integrated luminosity of the data sample is $\mathcal{L} = 4630 \pm 208$ pb^{-1}, and the branching ratio $BR(WW \to \ell\nu) = 0.1080 \pm 0.0009$ [1].

Sample	Total Yield ± stat ± syst	$ee/\mu\mu$	$e\mu/\mu e$
$qqWW$	728.40 ± 4.11 ± 43.42	279.29 ± 2.55 ± 16.65	449.10 ± 3.23 ± 26.77
$ggWW$	43.22 ± 0.58 ± 13.20	16.65 ± 0.36 ± 5.08	26.57 ± 0.46 ± 8.11
$t\bar{t} + tW$	125.27 ± 2.26 ± 24.43	45.13 ± 1.35 ± 8.80	80.14 ± 1.81 ± 15.63
$W + jets$	59.61 ± 3.93 ± 21.46	16.40 ± 2.28 ± 5.91	43.21 ± 3.20 ± 15.55
WZ/ZZ	27.37 ± 0.42 ± 2.02	17.05 ± 0.36 ± 1.16	10.32 ± 0.22 ± 1.01
$Z/\gamma*$	12.72 ± 3.44 ± 5.47	12.72 ± 3.44 ± 5.47	0.00 ± 0.00 ± 0.00
$W\gamma*/W+\gamma$	18.62 ± 3.18 ± 4.38	4.97 ± 1.31 ± 1.17	13.64 ± 2.90 ± 3.21
Total Bkgd.	244.31 ± 6.54 ± 33.32	96.27 ± 4.55 ± 12.04	148.04 ± 4.69 ± 22.30
Total Bkgd.+Signal	1015.93 ± 7.75 ± 56.52	392.21 ± 5.23 ± 21.24	623.72 ± 5.71 ± 35.91
Data	1130	462	668

Table 13: Expected number of signal and background events from the data-driven methods for an integrated luminosity of 4.63 fb^{-1}after applying the selection requirements.

Using the inputs described previously and Equation 16, we obtain the following WW cross-section measurement:

$$\sigma_{WW} = 53.41 \pm 2.03 \text{ (stat.)} \pm 4.28 \text{ (syst.)} \pm 2.40 \text{ (lumi.) pb.}$$

8 Summary

We have performed a measurement of the W^+W^- production cross-section using an integrated luminosity of 4.63 fb^{-1} of pp collision data at $\sqrt{s} = 7$ TeV. The measurement was performed in the $W^+W^- \to \ell^+\nu\ell^-\bar{\nu}$ final state. The W^+W^- production cross-section was measured to be:

$$\sigma_{WW} = 53.41 \pm 2.03 \text{ (stat.)} \pm 4.28 \text{ (syst.)} \pm 2.40 \text{ (lumi.) pb,}$$

to be compared with the standard model prediction [49]:

$$\sigma_{WW} = 47 \pm 2 \text{ pb.}$$

References

[1] K. Nakamura et al. (Particle Data Group), "Review of particle physics", J. Phys.G37 , 2010.

[2] F. Englert and R. Brout, "Broken symmetries and the masses of gauge bosons", Phys. Rev. Lett. 13, 1964.

[3] P. W. Higgs, "Broken symmetry and the mass of gauge vector mesons", Phys. Rev. Lett. 13, 1964.

[4] Guralnik, G.S. and Hagen, C.R. and Kibble, T.W.B., "Global Conservation Laws and Massless Particles", Phys.Rev.Lett. 13, 1964.

[5] M. Dittmar and H. K. Dreiner, Phys. Rev. D **55** (1997) 167".

[6] CMS Collaboration, "Measurement of WW Production and Search for the Higgs Boson in pp Collisions at $\sqrt{s} = 7$ TeV", arXiv:1102.5429.

[7] W. Andrews, et al., A Higgs Boson Search in the Fully Leptonic W^+W^- Final State, CMS AN-2011/155 (2011).

[8] W. Andrews, et al., A Higgs Boson Search in the Fully Leptonic W^+W^- Final State with the Full 2011 Dataset, CMS AN-2011/456 (2011).

[9] F. Stoeckli, "http://indico.cern.ch/getFile.py/access?contribId=0&resId=1&materialId=slides&confId=49009", EWK Diboson meeting of March 12 2009.

[10] /afs/cern.ch/cms/CAF/CMSCOMM/COMM_DQM/certification/Collisions11/7TeV/Prompt/Cert_160404-163869_7TeV_PromptReco_Collisions11_JSON.txt.

[11] A. Vartak, M. LeBourgeois, V. Sharma, "Lepton Isolation in the CMS Tracker, ECAL and HCAL", CMS AN-2010/106.

[12] S. Xie, *et al.*, "Electron Identification Using Multivariate Methods", CMS AN-2011/413.

[13] W. Erdmann, M. LeBourgeois, B. Mangano, https://indico.cern.ch/getFile.py/access?contribId=5&sessionId=3&resId=1 note in preparation.

[14] B. Mangano *et al.*, "Improvement in Photon Conversion Rejection Performance Using Advanced Tracking Tools", AN-10-283.

[15] S. Xie, *et al.*", "Study of Data-Driven Methods for Estimation of Fake Lepton Backgrounds", CMS AN-2009/120.

[16] W. Andrews, *et al.*, "Fake Rates for dilepton Analyses", CMS AN-2010/257.

[17] F. Golf, D. Evans, J. Mulmenstadt *et al.*, "Expectations for observation of top quark pair production in the dilepton final state with the early CMS data", CMS AN-2009/050.

[18] W. Andrews, et al., A Method to Measure the Contribution of $Z/\gamma^* \to \ell\ell$ to a di-lepton+ MET Selection, CMS AN-2009/023 (2009).

[19] CMS Collaboration, "Jet Energy Calibration with Photon+Jet Events", PAS JME-09-004.

[20] CMS Collaboration, "Jet Performance in pp Collisions at $\sqrt{s} = 7$ TeV", PAS JME-10-003.

[21] CMS collaboration, "Commissioning of b-jet identification with pp collisions at $\sqrt{s} = 7$ TeV, BTV-10-001.

[22] Cacciari, Matteo and Salam, Gavin P. and Soyez, Gregory, "The anti-k_t jet clustering algorithm", JHEP 04, 2008.

[23] W. Andrews, *et al.*, "Study of photon conversion rejection at CMS", CMS AN-2009/159.

[24] A. Hoecker, *et al.*, "TMVA - Toolkit for Multivariate Data Analysis", arXiv:physics/0703039, 2007.

[25] CMS Generator group, Standard Model Cross Sections for CMS at 7 TeV, 2010.

[26] PDF4LHC Working Group, `http://www.hep.ucl.ac.uk/pdf4lhc/PDF4LHCrecom.pdf`.

[27] Nadolsky, Pavel M. and others, "Implications of CTEQ global analysis for collider observables", Phys. Rev. D78 2008.

[28] Martin, A. D. and Stirling, W. J. and Thorne, R. S. and Watt, G., "Parton distributions for the LHC, Eur. Phys. J. C63 2009.

[29] Ball, Richard D. and others, "A first unbiased global NLO determination of parton distributions and their uncertainties", arXiv 1002.4407.

[30] A. O'Hagan and J.J. Forster, "Bayesian Inference", Kendall's Advanced Theory of Statistics, Arnold, London, 2B, 2004.

[31] G. Bauer *et. al.*, "Lepton ef?iencies for the inclusive W cross section measurement with 36.1pb^{-1}", AN2011/097.

[32] W. Andrews *et. al.*, "Uncertainties on the Lepton Selection Efficiency for t$\bar{t}$ Cross Section Analysis", AN2010/274.

[33] David Sabes, "Electron reconstruction efficiency", https://indico.cern.ch/getFile.py/access?contribId=2&resId=0&materialId=slides&confId=140397.

[34] LHC Higgs Cross Section Working Group, "Handbook of LHC Higgs Cross Sections: Inclusive Observables", CERN-2011-002, 2011.

[35] CMS Collaboration, "CMS MET Performance in Events Containing Electroweak Bosons from pp Collisions at $\sqrt{s} = 7$ TeV", CMS PAS JME-2010-005 (2010).

[36] M. Zanetti, "MET with PU in $H \to W^+W^- \to 2\ell 2\nu$", https://indico.cern.ch/conferenceDisplay.py?confId=131580; B. Hooberman, "MET with PU in MC and First 2011 Data", https://indico.cern.ch/contributionDisplay.py?contribId=5&confId=132579.

[37] Mingshui Chen and Andrey Korytov, https://mschen.web.cern.ch/mschen/lands/.

[38] J. Campbell, R.K. Ellis, G. Zanderighi, "Next-to-Leading order Higgs + 2 jet production via gluon fusion.", JHEP 0610:028 (2006), hep-ph/0608194.

[39] J. Campbell, R.K. Ellis, C. Williams, "Vector boson pair production at the LHC.", arxiv:hep-ph/1105.0020.

[40] M. Plummer, "Jet Another Gibbs Sampler", http://www-ice.iarc.fr/m̃artyn/software/jags/.

[41] W. Andrews *et. al.*, "Shape analysis for Higgs searches in di-lepton final state", CMS AN2011/408.

[42] J. Campell, F. Tramontano, "Next-to-leading order corrections to Wt production and decay", arxiv:hep-ph/0506289.

[43] C.D. White, S. Frixione, E. Leanen, F. Maltoni *et. al.*, "Isolating Wt production at the LHC", arxiv:hep-ph/0908.0631.

[44] R. C. Gray, C. Kilic, M. Park, S. Somalwar and S. Thomas, "Backgrounds To Higgs Boson Searches from Asymmetric Internal Conversion", arXiv:1110.1368 [hep-ph].

[45] T. Junk, "Confidence level computation for combining searches with small statistics", Nucl.Instrum.Meth. **A434** (1999) 435443, arXiv:hep-ex/9902006. doi:10.1016/S0168-9002(99)00498-2.

[46] A. L. Read, "Modified frequentist analysis of search results (the CLs method)", CERN Yellow Report CERN-2000-005 (2000) 81.

[47] ATLAS Collaboration, CMS Collaboration, and LHC Higgs Combination Group, "Procedure for the LHC Higgs boson search combination in summer 2011", (July, 2011)

[48] W. Andrews, et al.,"Jet-veto Efficiency for the WW production cross section in pp collisions at $sqrts = 7$ TeV",CMS AN-2010/385 (2010).

[49] J. M. Campbell, R. K. Ellis and C. Williams, JHEP **1107**, 018 (2011) [arXiv:1105.0020 [hep-ph]].

Appendices

A Fake Rate Studies

A.1 Muon Fake Rate

We summarize the muon fake rate measurements in this appendix section. We use the same fakeable object definition described in reference [7]. Also an analogous trigger selection is used.

A.1.1 Muon Fake Rate Results

The muon fake rates measured for the full 2011 data requiring the leading jet p_T to be larger than 15 GeV are shown in Figure 4 as a function of the p_T and η of the muon. The fake rates are tabulated in the p_T and η bins used to perform the background estimate in Table 14.

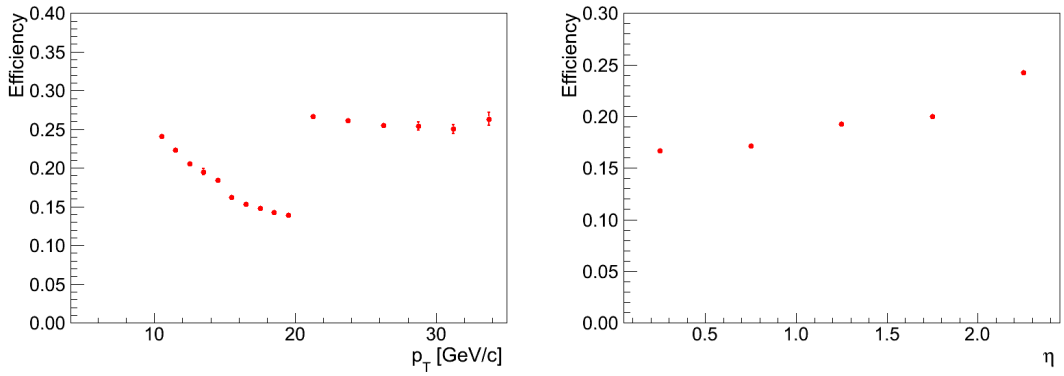

(a) p_T (b) η

Figure 4: Muon fake rates as a function for p_T and η for the full 2011 dataset.

	$0 < \eta < 1.0$	$1.0 < \eta < 1.479$	$1.479 < \eta < 2.0$	$2.0 < \eta < 2.5$
$10 < p_T <= 15$	$0.197 +/- 0.002$	$0.212 +/- 0.003$	$0.230 +/- 0.003$	$0.267 +/- 0.004$
$15 < p_T <= 20$	$0.137 +/- 0.001$	$0.156 +/- 0.001$	$0.172 +/- 0.001$	$0.209 +/- 0.003$
$20 < p_T <= 25$	$0.254 +/- 0.002$	$0.289 +/- 0.003$	$0.254 +/- 0.003$	$0.309 +/- 0.006$
$25 < p_T <= 30$	$0.240 +/- 0.004$	$0.275 +/- 0.006$	$0.253 +/- 0.006$	$0.298 +/- 0.011$
$30 < p_T <= 35$	$0.237 +/- 0.006$	$0.271 +/- 0.010$	$0.257 +/- 0.010$	$0.328 +/- 0.021$

Table 14: Muon fake rate in η-p_T using the full 2011 data. Uncertainties are statistical only. A combination of the **Mu8**, **Mu15**, and **kHLT_Mu8_Jet40** triggers are used, with a p_T threshold on the leading jet in the event of 15 GeV.

A.1.2 Pileup Dependence

Due to the effect of energy from pileup interactions on the electron isolation, there can be a small dependence of the fake rate on the number of reconstructed primary vertices. From Figure 5 we observe that the pileup dependence is negligible.

A.2 Electron Fake Rate

We summarize the electron fake rate measurements in this appendix section. We use the same fakeable object definition described in reference [7]. Also an analogous trigger selection is used.

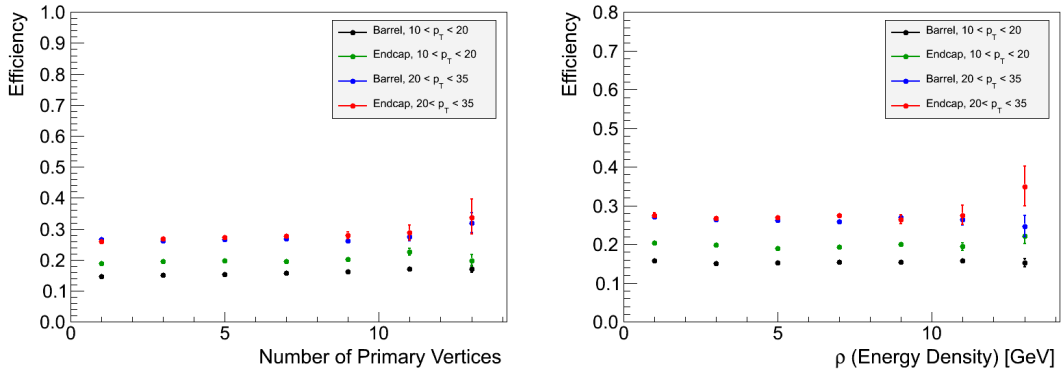

(a) Number of Reconstructed Primary Vertices (b) Pileup Energy Density (ρ)

Figure 5: Muon fake rates as a function of the number of reconstructed primary vertices (a) and the pileup energy density (b) in four different p_T and η bins.

A.2.1 Trigger Bias

Due to the evolving trigger menu, the requirements on the electron legs of the electron muon triggers and the double electron triggers are different for different run ranges. Essentially three different levels of requirements are imposed:

- HLT Electron (HLT_Ele8),
- CaloIdL CaloIsoVL (HLT_Ele8_CaloIdL_CaloIsoVL),
- CaloIdT TrkIdVL CaloIsoVL TrkIsoVL (HLT_Ele8_CaloIdT_TrkIdVL_CaloIsoVL_TrkIsoVL).

In Figure 6 we verify that the different trigger requirements do not result in a bias of the electron fake rate, in the nominal fake rate measurement sample with a leading jet p_T cut of 35 GeV and the sample with a leading jet p_T cut of 15 GeV where statistical uncertainties are much smaller. As a result we can use all fake rate trigger samples and perform a combined fake rate measurement which can be applied to all final states.

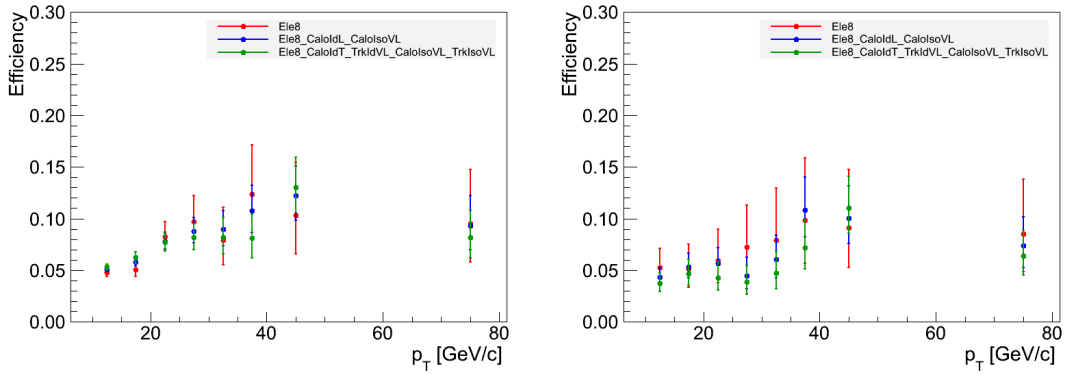

(a) (b)

Figure 6: Electron fake rates as a function for p_T for different trigger samples.

A.2.2 Electron Fake Rate Results

The electron fake rates measured for the full 2011 data requiring the leading jet p_T to be larger than 35 GeV are shown in Figure 7 as a function of the p_T and η of the electron. The fake rates are tabulated in the p_T and η bins used to perform the background estimate in Table 15.

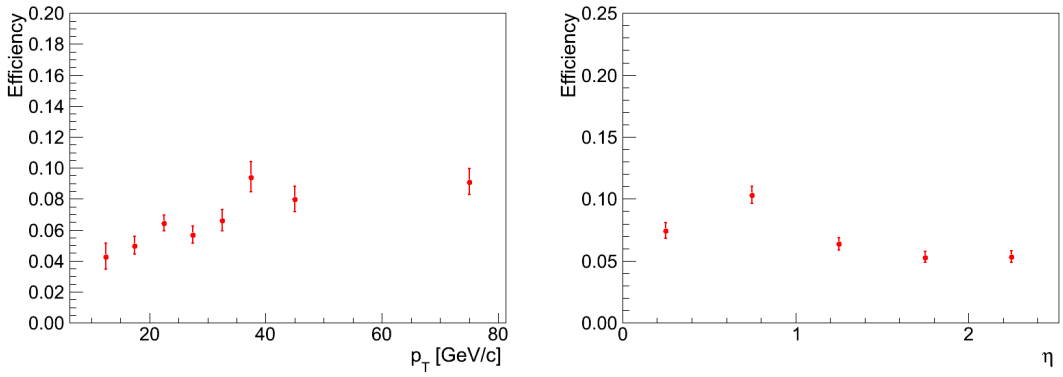

(a) p_T (b) η

Figure 7: Electron fake rates as a function for p_T and η for the full 2011 dataset.

	$0 < \eta < 1.0$	$1.0 < \eta < 1.479$	$1.479 < \eta < 2.0$	$2.0 < \eta < 2.5$
$10 < p_T <= 15$	$0.070 +/- 0.010$	$0.037 +/- 0.008$	$0.023 +/- 0.007$	$0.030 +/- 0.009$
$15 < p_T <= 20$	$0.075 +/- 0.009$	$0.043 +/- 0.008$	$0.016 +/- 0.005$	$0.038 +/- 0.009$
$20 < p_T <= 25$	$0.088 +/- 0.009$	$0.064 +/- 0.009$	$0.049 +/- 0.008$	$0.042 +/- 0.007$
$25 < p_T <= 30$	$0.080 +/- 0.009$	$0.054 +/- 0.010$	$0.035 +/- 0.007$	$0.066 +/- 0.010$
$30 < p_T <= 35$	$0.078 +/- 0.011$	$0.085 +/- 0.014$	$0.073 +/- 0.012$	$0.051 +/- 0.010$

Table 15: Electron fake rate in η-p_T using the full 2011 data. Uncertainties are statistical only. A combination of the **Ele8_CaloIdL_CaloIsoVL**, **Ele17_CaloIdL_CaloIsoVL**, **Ele8_CaloIdL_CaloIsoVL_Jet40**, and **HLT_Ele8_CaloIdT_TrkIdVL_CaloIsoVL_TrkIsoVL** triggers are used, with a p_T threshold on the leading jet in the event of 35 GeV.

A.2.3 Pileup Dependence

Due to the effect of energy from pileup interactions on the electron isolation, there is a small dependence of the fake rate on the number of reconstructed primary vertices shown in Figure 8.

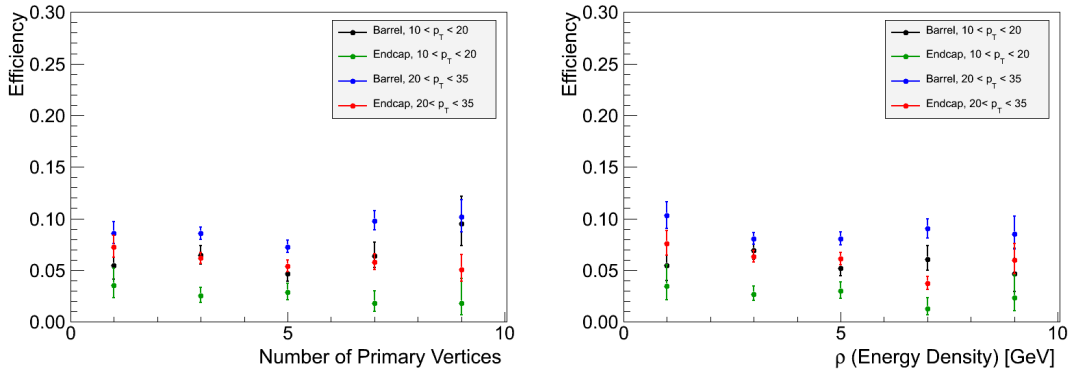

(a) Number of Reconstructed Primary Vertices

(b) Pileup Energy Density (ρ)

Figure 8: Electron fake rates as a function of the number of reconstructed primary vertices (a) and the pileup energy density (b) in four different p_T and η bins.

	$0 < \eta < 1.0$	$1.0 < \eta < 1.479$	$1.479 < \eta < 2.0$	$2.0 < \eta < 2.5$
$10 < p_T <= 15$	$0.091 +/- 0.035$	$0.016 +/- 0.016$	$0.016 +/- 0.016$	$0.067 +/- 0.037$
$15 < p_T <= 20$	$0.055 +/- 0.024$	$0.043 +/- 0.025$	$0.033 +/- 0.023$	$0.050 +/- 0.028$
$20 < p_T <= 25$	$0.091 +/- 0.026$	$0.051 +/- 0.025$	$0.049 +/- 0.024$	$0.000 +/- 0.000$
$25 < p_T <= 30$	$0.094 +/- 0.030$	$0.127 +/- 0.045$	$0.025 +/- 0.017$	$0.042 +/- 0.024$
$30 < p_T <= 35$	$0.096 +/- 0.034$	$0.018 +/- 0.017$	$0.141 +/- 0.043$	$0.083 +/- 0.040$

Table 16: Electron fake rate in η-p_T using the full 2011 data in events with 1 or 2 reconstructed primary vertices. Uncertainties are statistical only. A combination of the **Ele8_CaloIdL_CaloIsoVL**, **Ele17_CaloIdL_CaloIsoVL**, **Ele8_CaloIdL_CaloIsoVL_Jet40**, and **HLT_Ele8_CaloIdT_TrkIdVL_CaloIsoVL_TrkIsoVL** triggers are used, with a p_T threshold on the leading jet in the event of 35 GeV.

	$0 < \eta < 1.0$	$1.0 < \eta < 1.479$	$1.479 < \eta < 2.0$	$2.0 < \eta < 2.5$
$10 < p_T <= 15$	$0.071 +/- 0.014$	$0.027 +/- 0.010$	$0.023 +/- 0.010$	$0.031 +/- 0.012$
$15 < p_T <= 20$	$0.073 +/- 0.012$	$0.046 +/- 0.012$	$0.007 +/- 0.005$	$0.048 +/- 0.014$
$20 < p_T <= 25$	$0.065 +/- 0.011$	$0.079 +/- 0.014$	$0.047 +/- 0.011$	$0.048 +/- 0.011$
$25 < p_T <= 30$	$0.085 +/- 0.014$	$0.043 +/- 0.013$	$0.029 +/- 0.009$	$0.079 +/- 0.015$
$30 < p_T <= 35$	$0.058 +/- 0.013$	$0.109 +/- 0.023$	$0.067 +/- 0.016$	$0.055 +/- 0.016$

Table 17: Electron fake rate in η-p_T using the full 2011 data in events with 3, 4, or 5 reconstructed primary vertices. Uncertainties are statistical only. A combination of the **Ele8_CaloIdL_CaloIsoVL**, **Ele17_CaloIdL_CaloIsoVL**, **Ele8_CaloIdL_CaloIsoVL_Jet40**, and **HLT_Ele8_CaloIdT_TrkIdVL_CaloIsoVL_TrkIsoVL** triggers are used, with a p_T threshold on the leading jet in the event of 35 GeV.

	$0 < \eta < 1.0$	$1.0 < \eta < 1.479$	$1.479 < \eta < 2.0$	$2.0 < \eta < 2.5$
$10 < p_T <= 15$	$0.063 +/- 0.015$	$0.059 +/- 0.017$	$0.027 +/- 0.012$	$0.017 +/- 0.012$
$15 < p_T <= 20$	$0.086 +/- 0.015$	$0.037 +/- 0.013$	$0.020 +/- 0.010$	$0.021 +/- 0.012$
$20 < p_T <= 25$	$0.112 +/- 0.016$	$0.045 +/- 0.013$	$0.049 +/- 0.013$	$0.048 +/- 0.013$
$25 < p_T <= 30$	$0.068 +/- 0.014$	$0.051 +/- 0.016$	$0.043 +/- 0.013$	$0.060 +/- 0.016$
$30 < p_T <= 35$	$0.097 +/- 0.020$	$0.085 +/- 0.023$	$0.058 +/- 0.018$	$0.034 +/- 0.014$

Table 18: Electron fake rate in η-p_T using the full 2011 data in events with 6 or more reconstructed primary vertices. Uncertainties are statistical only. A combination of the **Ele8_CaloIdL_CaloIsoVL**, **Ele17_CaloIdL_CaloIsoVL**, **Ele8_CaloIdL_CaloIsoVL_Jet40**, and **HLT_Ele8_CaloIdT_TrkIdVL_CaloIsoVL_TrkIsoVL** triggers are used, with a p_T threshold on the leading jet in the event of 35 GeV.

B Cross Section Measurement Per Lepton Channel

We now calculate the W^+W^- production cross section in each lepton channel separately, according to equation 16. In all cases, the integrated luminosity of the data sample is taken to be $\mathcal{L} = 4630 \pm 208 \text{pb}^{-1}$, and the branching ratio $BR(WW \to \ell\nu) = 0.1080 \pm 0.0009$ [1]. The efficiency to select $\sigma_{WW \to 2\ell 2\nu}$ candidates, ε, is computed as the weighted mean of the $qq \to W^+W^-$ and $gg \to W^+W^-$ efficiencies in simulation, assuming a 3% contribution from the gg process.

The results are tabulated in the following sub-sections, and summarised in Figure 9.

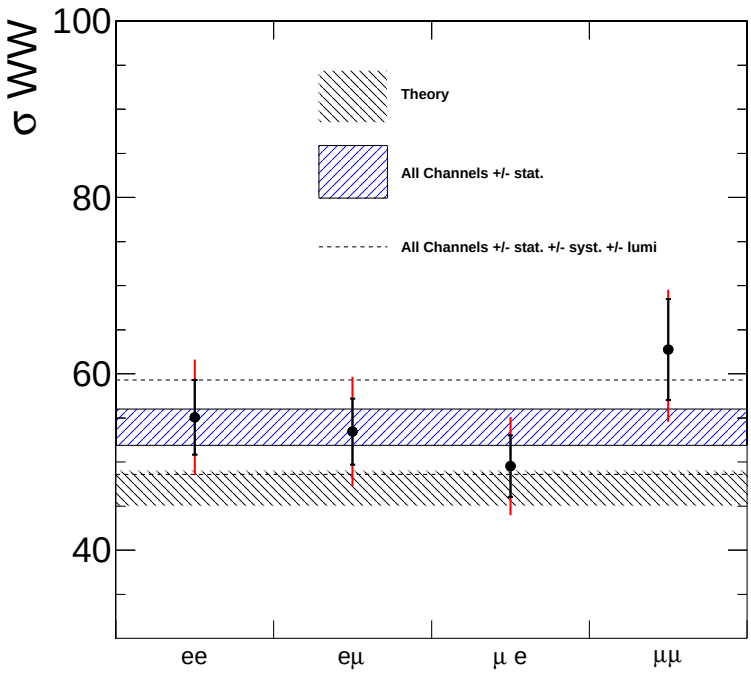

Figure 9: The cross section measured in each lepton channel compared to the nominal result combining all channels and the theoretical prediction.

B.1 *ee* Channel

The number of events observed and the background predictions and their uncertainties are given in Table 19. The signal efficiency, $\varepsilon = 0.00788 \pm 0.00055$. We obtain the following WW cross-section measurement:

$$\sigma_{WW} = 55.07 \pm 4.23 \text{ (stat.)} \pm 4.32 \text{ (syst.)} \pm 2.48 \text{ (lumi.) pb}$$

Sample	Yield ± stat ± syst
$qqWW$	170.1 ± 2.0 ± 10.7
$ggWW$	10.0 ± 0.3 ± 3.0
$t\bar{t} + tW$	28.3 ± 1.1 ± 5.5
$W + jets$	6.2 ± 2.0 ± 2.2
WZ/ZZ	10.5 ± 0.3 ± 0.7
$Z/\gamma*$	5.7 ± 2.2 ± 2.5
$W\gamma*/W+\gamma$	1.3 ± 0.8 ± 0.3
Total Bkgd.	52.0 ± 3.3 ± 6.5
Total Bkgd.+Signal	232.1 ± 3.8 ± 12.9
Data	263

Table 19: Expected number of signal and background events from the data-driven methods for an integrated luminosity of 4.63 fb^{-1}after applying the selection requirements in the ee channel.

B.2 $e\mu$ Channel

The number of events observed and the background predictions and their uncertainties are given in Table 20. The signal efficiency, $\varepsilon = 0.00979 \pm 0.00069$. We obtain the following WW cross-section measurement:

$$\sigma_{WW} = 53.45 \pm 3.75 \text{ (stat.)} \pm 4.31 \text{ (syst.)} \pm 2.41 \text{ (lumi.) pb}$$

Sample	Yield ± stat ± syst
$qqWW$	210.8 ± 2.2 ± 13.3
$ggWW$	12.8 ± 0.3 ± 3.9
$t\bar{t} + tW$	38.1 ± 1.3 ± 7.4
$W + jets$	15.4 ± 1.8 ± 5.5
WZ/ZZ	4.2 ± 0.1 ± 0.4
$Z/\gamma*$	0.0 ± 0.0 ± 0.0
$W\gamma*/W+\gamma$	6.8 ± 2.7 ± 1.5
Total Bkgd.	64.7 ± 3.5 ± 9.4
Total Bkgd.+Signal	288.3 ± 4.1 ± 16.7
Data	319

Table 20: Expected number of signal and background events from the data-driven methods for an integrated luminosity of 4.63 fb^{-1}after applying the selection requirements in the $e\mu$ channel.

B.3 μe Channel

The number of events observed and the background predictions and their uncertainties are given in Table 21. The signal efficiency, $\varepsilon = 0.01103 \pm 0.00078$. We obtain the following WW cross-section measurement:

$$\sigma_{WW} = 49.54 \pm 3.48 \text{ (stat.)} \pm 3.74 \text{ (syst.)} \pm 2.23 \text{ (lumi.) pb}$$

B.4 $\mu\mu$ Channel

The number of events observed and the background predictions and their uncertainties are given in Table 22. The signal efficiency, $\varepsilon = 0.00507 \pm 0.00036$. We obtain the following WW cross-section measurement:

$$\sigma_{WW} = 62.76 \pm 5.72 \text{ (stat.)} \pm 5.18 \text{ (syst.)} \pm 2.82 \text{ (lumi.) pb}$$

Sample	Yield ± stat ± syst
$qqWW$	238.3 ± 2.4 ± 15.0
$ggWW$	13.8 ± 0.3 ± 4.2
$t\bar{t} + tW$	42.1 ± 1.3 ± 8.2
$W + jets$	27.8 ± 2.6 ± 10.0
WZ/ZZ	6.1 ± 0.2 ± 0.6
$Z/\gamma*$	0.0 ± 0.0 ± 0.0
$W\gamma*/W+\gamma$	6.9 ± 1.2 ± 2.0
Total Bkgd.	83.3 ± 3.3 ± 6.5
Total Bkgd.+Signal	335.4 ± 4.1 ± 16.9
Data	349

Table 21: Expected number of signal and background events from the data-driven methods for an integrated luminosity of 4.63 fb^{-1}after applying the selection requirements in the μe channel.

Sample	Yield ± stat ± syst
$qqWW$	109.2 ± 1.6 ± 6.9
$ggWW$	6.7 ± 0.2 ± 2.0
$t\bar{t} + tW$	16.8 ± 0.8 ± 3.3
$W + jets$	10.2 ± 1.1 ± 3.7
WZ/ZZ	6.5 ± 0.2 ± 0.5
$Z/\gamma*$	7.0 ± 2.7 ± 3.0
$W\gamma*/W+\gamma$	3.7 ± 1.0 ± 1.0
Total Bkgd.	44.2 ± 3.1 ± 5.9
Total Bkgd.+Signal	160.1 ± 3.5 ± 9.3
Data	199

Table 22: Expected number of signal and background events from the data-driven methods for an integrated luminosity of 4.63 fb^{-1}after applying the selection requirements in the $\mu\mu$ channel.